

RESEARCH ARTICLE

Carvedilol inhibits neuronal hyperexcitability caused by epilepsy-associated KCNT1 mutations

Chang Di^{1,2} | Tong Wu¹ | Kai Gao^{3,4,5,6} | Na Li¹ | Huifang Song¹ |
 Lili Wang¹ | Haojie Sun⁷ | Jingyun Yi¹ | Xinran Zhang¹ | Jiexin Chen¹ |
 Mala Shah⁷ | Yuwu Jiang^{3,4,5,6} | Zhuo Huang^{1,8} 

¹State Key Laboratory of Natural and Biomimetic Drugs, Department of Molecular and Cellular Pharmacology, School of Pharmaceutical Sciences, Peking University Health Science Center, Beijing, China

²Department of Pharmacology, School of Basic Medical Sciences, Peking University Health Science Center; State Key Laboratory of Vascular Homeostasis and Remodeling, Peking University, Beijing, China

³Department of Pediatrics, Peking University First Hospital, Beijing, China

⁴Beijing Key Laboratory of Molecular Diagnosis and Study on Pediatric Genetic Diseases, Beijing, China

⁵Children Epilepsy Center, Peking University First Hospital, Beijing, China

⁶Key Laboratory for Neuroscience, Ministry of Education/National Health and Family Planning Commission, Peking University, Beijing, China

⁷UCL School of Pharmacy, University College London, London, UK

⁸IDG/McGovern Institute for Brain Research, Peking University, Beijing, China

Correspondence

Zhuo Huang, Department of Molecular and Cellular Pharmacology, Peking University Health Science Center, 38 Xue Yuan Road, Beijing 100191, China.
 Email: huangz@hsc.pku.edu.cn

Yuwu Jiang, Department of Pediatrics, Peking University First Hospital, No.1 Xi'an Men Street, West District, Beijing 100034, China.
 Email: jiangyuwu@bjmu.edu.cn

Mala Shah, Department of Pharmacology, School of Pharmacy, University College London, London WC1N 1AX, U.
 Email: mala.shah@ucl.ac.uk

Funding information

National Natural Science Foundation of China Grant, Grant/Award Numbers: 31871083, 81371432, U22A20339, 81971211, 82171435; Key Project of Clinical Medicine Research of National Clinical Research Center for Child Health and Disorders, Children's Hospital of Chongqing Medical University, Grant/Award Number: NCRCHD-2021-KP-02; National Key Research and Development Program of China, Grant/Award Number: 2020YFA0804000; Beijing Natural Science Foundation, Grant/Award Number: 7212109;

Background and Purpose: *KCNT1* encodes a sodium-activated potassium channel (Slack channel), and its mutation can cause several forms of epilepsy. Traditional anti-epileptic medications have limited efficacy in treating patients with *KCNT1* mutations. Here, we describe one heterozygous *KCNT1* mutation, M267T, in a patient with EIMFS. The pathological channel properties of this mutation and its effect on neuronal excitability were investigated. Additionally, this study aimed to develop a medication for effective prevention of *KCNT1* mutation-induced seizures.

Experimental Approach: Wild-type or mutant *KCNT1* plasmids were expressed heterologously in *Xenopus laevis* oocytes, and channel property assessment and drug screening were performed based on two-electrode voltage-clamp recordings. The single-channel properties were investigated using the excised inside-out patches from HEK293T cells. Through in utero electroporation, WT and M267T Slack channels were expressed in the hippocampal CA1 pyramidal neurons in male mice, followed by the examination of the electrical properties using the whole-cell current-clamp technique. The kainic acid-induced epilepsy model in male mice was used to evaluate the antiseizure effects of carvedilol.

Key Results: The *KCNT1* M267T mutation enhanced Slack channel function by increasing single-channel open probability. Through screening 16 FDA-approved ion channel blockers, we found that carvedilol effectively reversed the mutation-induced

Abbreviations: ADNFLE, autosomal dominant nocturnal frontal lobe epilepsy; ADP, depolarizing afterpotential; AHP, afterhyperpolarization; AP, action potential; ASMs, anti-aeizure medications; EIMFS, epilepsy of infancy with migrating partial seizures of infancy; GOF, Gain-of-function; IUE, in utero electroporation; KA, Kainic acid; K_{Na} currents, sodium activated potassium currents; mAHP, medium afterhyperpolarization; sAHP, slow afterhyperpolarization; Slack channel, Sequence like a calcium-activated K^+ channel; WT, wild type.

Chang Di, Tong Wu, Kai Gao and Na Li contributed equally.

Chinese National Programs for Brain Science and Brain-like intelligence technology, Grant/Award Number: 2021ZD0202102

gain-of-function channel properties. Notably, the KCNT1 M267T mutation in the mouse hippocampal CA1 pyramidal neurons affected afterhyperpolarization properties and induced neuronal hyperexcitability, which was inhibited by carvedilol. Additionally, carvedilol exhibited antiseizure effects in the kainic acid-induced epilepsy model.

Conclusion and Implication: Our findings suggest carvedilol as a new potential candidate for treatment of epilepsies.

KEYWORDS

afterhyperpolarization, carvedilol, epilepsy, KCNT1

1 | INTRODUCTION

The gene *KCNT1* encodes a sodium-activated potassium channel (also known as the Slack channel, sequence like a calcium-activated K⁺ channel, Slo2.2 or *K_{Na}1.1*), which is highly expressed in various regions of the mammalian brain, especially in the cerebral cortex, hippocampus and cerebellum (Bhattacharjee et al., 2002; Shore et al., 2020; Yuan et al., 2003). The Slack channels regulate sodium-activated potassium currents (*K_{Na}* currents), which regulate neuronal firing patterns by modifying the afterdepolarization (ADP) and afterhyperpolarization (AHP) currents under normal physiological conditions (Franceschetti et al., 2003; Hess et al., 2007; Liu & Stan Leung, 2004; Quraishi et al., 2019; Schwandt et al., 1989; Shore et al., 2020). Additionally, the *K_{Na}* currents regulate the neuronal bursting (Lu et al., 2015; Martinez-Espinosa et al., 2015) and maintain the timing accuracy of action potentials (APs) at high frequencies in the auditory brainstem neurons (Yang et al., 2007).

KCNT1 mutations are the most frequent genetic cause of epilepsy of infancy with migrating partial seizures of infancy (EIMFS), an incurable and intractable infantile form of epilepsy, characterized by migrating multifocal seizures with onset before 6 months of age. Additionally, the patients present progressive developmental delay (Barcia et al., 2012; Coppola et al., 1995; Heron et al., 2012; Ishii et al., 2013; León-Ruiz et al., 2024; Møller et al., 2015; Shimada et al., 2014). The mortality rate of EIMFS is approximately 50%, with reported sudden unexpected death in epilepsy (Kuchenbuch et al., 2019; Møller et al., 2015). Other forms of focal epilepsy and epileptic encephalopathies, including autosomal dominant nocturnal frontal lobe epilepsy (ADNFLE), Ohtahara syndrome, and West Syndrome, have also presented *KCNT1* mutations (Heron et al., 2012; Martin et al., 2014).

Most epilepsy-related *KCNT1* mutations can increase the Slack current amplitudes (Barcia et al., 2012; Kim et al., 2014; Martin et al., 2014; Mikati et al., 2015; Milligan et al., 2014). This gain-of-function (GOF) in Slack channels induced neuronal hyperexcitability in human induced pluripotent stem cell-derived neurons (Quraishi et al., 2019). Additionally, *KCNT1*^{+R455H} mice have been shown to exhibit persistent interictal spikes, spontaneous seizures, considerably increased sensitivity to pentylenetetrazol and increased mortality following seizures (Quraishi et al., 2020).

What is already known?

- *KCNT1* mutations can cause several forms of epilepsy.
- Traditional antiepileptic medications have limited efficacy in treating patients with *KCNT1* mutations.

What does this study add?

- The clinical phenotype and pathologic channel properties of *KCNT1* M267T mutation have been identified.
- Carvedilol reduces Slack current, neuronal excitability, and seizure susceptibility in a mouse epilepsy model.

What is the clinical significance?

- Carvedilol may be a new potential candidate for the treatment of epilepsies.

To date, no effective treatments have been established for *KCNT1*-related epilepsies. **Quinidine**, a class I anti-arrhythmic drug, has been applied clinically in patients with *KCNT1*-related epilepsies, as it could reverse the Slack channel overactivity in vitro (Bearden et al., 2014; Milligan et al., 2014). However, owing to its variable dosing, serum concentrations and off-target effects, quinidine is not generally effective (Mullen et al., 2018; Numis et al., 2018). The clinical severity of *KCNT1*-related epilepsies warrants research on exploring *KCNT1*-targeting drugs as novel therapeutic strategies for epilepsy management.

Here, we have identified a heterozygous *KCNT1* mutation, M267T, with descriptions of its clinical phenotype and pathophysiological channel properties. To investigate how M267T Slack mutation contributes to neuronal excitability, we generated a mouse model carrying the M267T Slack channel in hippocampal CA1 pyramidal neurons, using in utero electroporation (IUE), and characterized electrophysiological properties of these neurons with electrophysiological recordings. Additionally, a number of FDA-approved

compounds were screened to identify compounds able to reduce whole-cell Slack current- and neuronal excitability, and thus to lower the seizure susceptibility in a mouse model of kainic acid (KA)-induced epilepsy.

2 | METHODS

2.1 | Patient data

Written informed consent was obtained from the parents of the patient. This study was approved by Peking University Institutional Review Board. We retrospectively summarised and analysed other patient data including seizure onset, seizure types, EEG and MRI findings, and response to clinical treatment with anti-seizure medications (ASMs) and quinidine.

2.2 | Genetic analysis

The proband was identified by next generation sequencing (NGS) using a gene panel targeting 480 epilepsy-related genes that included *KCNT1*. This panel used the Agilent SureSelect Target Enrichment technique, containing a total of 11,417 probes covering 1.285 Mbp. Targeted NGS was subsequently performed on an Illumina GAIIX platform using paired-end sequencing of 110 bp to screen for variants. Image analysis and base calling were performed by RTA software and CASAVA software v1.8.2 (Illumina, Cambridge, UK). After marking duplicate reads and removing reads of low base quality score using the Genome Analysis Tool Kit (GATK), clean paired-end reads were aligned to GRCh37/hg19 using BWA software (Pittsburgh Supercomputing Center, Pittsburgh, PA, USA). Then insertion-deletions (indels) and single-nucleotide polymorphisms (SNPs) identified using the GATK. Variants were annotated by ANNOVAR. We performed validation and parental origin analyses for the mutation by Sanger sequencing.

2.3 | Animals

All animal care and experimental procedures were in strict accordance with the 'Guide for the Care and Use of Laboratory Animals' and the 'Principles for the Utilization and Care of Vertebrate Animals', and were approved by the Institutional Animal Care and Use Committee at Peking University. Animal studies are reported in compliance with the ARRIVE guidelines (Percie du Sert et al., 2020) and with the recommendations made by the *British Journal of Pharmacology* (Lilley et al., 2020).

C57BL/6 male mice (6–8 weeks, 18–23 g) were purchased from Charles River Laboratories (Beijing, China). All mice were kept in specific pathogen-free conditions and maintained in a room at constant temperature ($24 \pm 2^\circ\text{C}$) and humidity (45%) on a 12-hr light/dark cycle with free access to food and water. Three or four mice were kept in one cage.

The experimenters were blinded to viral treatment or drug treatments during behavioural testing. Electrophysiological recordings and anatomical investigation were all performed in the dorsal part of the hippocampus.

2.4 | Cell culture

Human embryonic kidney (HEK) 293T cells (ATCC, Cat# CRL-3216, RRID: CVCL_0063) were cultured in Dulbecco's modified Eagle's medium supplemented with 10% fetal bovine serum at 37°C with 5% CO_2 . The HEK293T cells were passaged at 2–3 day intervals.

2.5 | Site-directed mutagenesis and cRNA synthesis

Human *KCNT1* (Genbank: NM_020822.2) were synthesized by GenScript (Nanjing, China). The expression constructs were produced by inserting the WT and mutated *KCNT1* coding sequences into the pcDNA3.1 (+) vector between restriction sites NheI and EcoRI. Site-directed mutagenesis of the *KCNT1* construct was performed using the QuikChange II XL Site-Directed Mutagenesis Kit (Agilent, Santa Clara, CA, USA) with the primers listed in Table S1. Construct fidelity was confirmed by DNA sequencing. The cDNA construct was then linearized using NotI, and the complementary RNA (cRNA) was synthesized using the mMACHINE T7 transcription kit (Thermo Fisher Scientific (Waltham, MA, USA)). RNA purity and concentration were checked using a Nanodrop reader. RNA quality was also checked on a 1% formaldehyde agarose gel. cRNA was stored at -80°C until ready for use.

2.6 | Electrophysiological characterization in *Xenopus* oocytes

Xenopus oocytes were surgically removed from *Xenopus laevis*. Stage V-VII oocytes were treated with $2\text{ mg}\cdot\text{ml}^{-1}$ of collagenase type I (Sigma Aldrich, St. Louis, MO, USA) in Ca^{2+} -free saline solution (96-mM NaCl, 2-mM KCl, 5-mM MgCl_2 and 5-mM HEPES, pH 7.6) for 0.5–1 h at room temperature. Oocytes were later microinjected with 23 nl of sterile water containing 10 ng of RNA encoding wild-type *KCNT1* or *KCNT1* mutants or with water alone. The injected oocytes were incubated for 1–3 days at 16°C in ND96 solution (96-mM NaCl, 2-mM KCl, 5-mM MgCl_2 , 1.8-mM CaCl_2 , 5-mM HEPES, 5-mM sodium pyruvate and $50\text{-}\mu\text{g}\cdot\mu\text{l}^{-1}$ gentamicin, pH 7.5). Whole-oocyte currents were measured by a two-electrode voltage clamp amplifier OC-725C (Warner Instruments, Holliston, MA, USA). Electrodes were filled with 3 M KCl and had resistances of 0.1–1.0 M Ω . Data were sampled at 1 kHz and filtered at 0.25 kHz. Data acquisition and analysis were carried out with Digidata 1322A (Axon Instruments Inc., Foster City, CA, USA) and pCLAMP software.

For measurements of channel activation, oocytes were held at -90 mV, and 500-ms duration test depolarizations were applied in 10 mV increments, from -80 to $+80$ mV, every 5 s. WT currents were always measured contemporaneously and with the same batch of oocytes with a mutant channel providing an internal control to address the possibility of batch-to-batch variation in expression. Quinidine, sodium valproate, levetiracetam and carbamazepine were dissolved in dimethyl sulfoxide (DMSO). All drugs were applied by continuous perfusion for 1 minute, then incubated for another 5 min, followed by a 10-min washout. Currents were recorded before application of compound, in the presence of compound, and following washout. Peak currents were measured at the end of each sweep for all clones. Statistical analysis was performed on Prism 6 (GraphPad Software, La Jolla, CA).

2.7 | Transient transfection and electrophysiological assessment

HEK293T cells were passaged 24 h before transfection, and plated on glass coverslips. Transient transfection was performed by adding 1–2 μ l of Lipofectamine 2000 (Invitrogen) and 1–2 μ g of human *KCNT1* plasmids. The mixture was added into a 35-mm cell culture dish. All cDNA clones were verified by sequencing. Patch clamp recordings were performed between 18 and 36 h after transfection.

Macroscopic currents of Slack channels were recorded in whole cell patch clamp configuration using a HEKA EPC10 amplifier driven by PatchMaster software. Patch pipettes were prepared from borosilicate glass and fire polished to resistance about 4.0 M Ω . For whole cell recordings, bath solution contained 140-mM NaCl, 5-mM KCl, 1-mM CaCl₂, 29-mM glucose and 10-mM HEPES (pH 7.4 with NaOH), pipette solution contained 100-mM K-gluconate, 30-mM KCl, 5-mM NaCl, 29-mM glucose, 5-mM EGTA and 10-mM HEPES (pH 7.3 with KOH). Membrane potential was held at -70 mV, and currents were elicited by a protocol consisting of a 400-ms step from -80 to $+80$ mV in 20-mV increments followed at 1-s intervals. For single channel recordings, bath solution contained 80-mM KCl, 40-mM NaCl, 2-mM MgCl₂, 1-mM EGTA, 10-mM HEPES, 20-mM choline chloride (pH 7.2 with KOH), pipette solution contained 140-mM KCl, 2-mM MgCl₂, 1-mM EGTA and 10-mM HEPES (pH 7.2 with KOH). Data are sampled at 20 kHz and low-pass filtered at 2.9 kHz. All patch clamp recordings were performed at room temperature and data were analysed with Igor Pro (WaveMetrics, Portland, OR USA) and Origin 8.6.

2.8 | Surface biotinylation

HEK-293T cells expressing *KCNT1* WT or M267T were incubated with 1 mg·ml⁻¹ of EZ-Link™ Sulfo-NHS-SS-Biotin (Thermo Fisher Scientific) in cold PBS for 1 h at 4°C, constantly moving. Free biotin was quenched, twice, with 100 mM Tris in cold PBS, and once with cold PBS to remove biotin excess. The cells were then harvested with GPCR Extraction Reagent (Pierce) and centrifuged at 15000g at 4°C

for 20 min. The supernatant was incubated with BeyoMag Streptavidin Magnetic Beads (Beyotime, Beijing, China), and the remaining supernatant was kept as input. The beads were subsequently washed with GPCR Extraction Reagent. The remaining proteins were eluted from the beads by re-suspending the beads in 1 \times SDS-PAGE loading buffer and incubating for 30 min at 37°C. The resultant materials were then subjected to western blot analysis.

2.9 | Western blot analysis

Proteins suspended in 1 \times SDS-PAGE loading buffer were denatured for 30 min at 37°C. Then proteins were loaded on 6% or 8% sodium dodecyl sulphate–polyacrylamide gel electrophoresis and transferred onto nitrocellulose filter membrane (PALL). Non-specific binding sites were blocked with Tris-buffered saline-Tween (0.02 M Tris, 0.137 M NaCl, and 0.1% Tween 20) containing 5% non-fat dried milk. Subsequently, proteins of interest were probed with primary antibodies for overnight at 4°C. After incubation with a secondary antibody, immunoreactive bands were visualized using HRP Substrate Peroxide Solution (Millipore, Billerica, MA, USA) according to the manufacturer's recommendation.

2.10 | In utero electroporation

Pregnant ICR mice on embryonic day 15 (E15) were anaesthetised with isoflurane, the intrauterine embryos were surgically manipulated as described previously (Tabata & Nakajima, 2001). Briefly, pcAGGS carrying wild-type or mutant *KCNT1* plasmids were purified without endotoxin. The concentration of the plasmid was adjusted to 2 mg·ml⁻¹. The plasmid containing 0.02% Fast Green solution was injected into the lateral ventricle of embryos at the indicated time. For targeting the hippocampus CA1 region, the angle of inclination of the electrode paddles with respect to horizontal plane of the brain was 250–275°. Square electric pulse (50 V for 50 ms) was passed five times at 950 ms intervals using an electroporator (NEPA GENE, Japan). After electroporation of all embryos the abdomen was sutured-closed, and embryos were let be born. The litters were processed for electrophysiological recordings at six postnatal weeks.

2.11 | Acute slice preparation and electrophysiological recordings

Horizontal slices containing dorsal hippocampus were obtained from 6-week-old mice electroporated of *KCNT1* plasmids. In accordance with previous studies (Huang et al., 2011), mice were anaesthetized with sodium pentobarbital and perfused intracardially with ice-cold 'cutting solution', then the brain was removed and submerged in ice-cold 'cutting solution' containing (mM): 110 choline chloride, 2.5 KCl, 0.5 CaCl₂, 7 MgCl₂, 25 NaHCO₃, 1.25 NaH₂PO₄ and 10 glucose; bubbled continuously with 95% O₂/5% CO₂ to maintain pH at 7.2. Next,

the brain was cut into 350 μm slices with a vibrating blade microtome (WPI, Sarasota, FL, USA). Slices were incubated in oxygenated (95% O_2 and 5% CO_2) 'recording solution' containing (mM): 125 NaCl, 2.5 KCl, 2 CaCl_2 , 2 MgCl_2 , 25 NaHCO_3 , 1.25 NaH_2PO_4 and 10 glucose (pH 7.4, 37°C) for 15 min, and then stored at room temperature in recording solution. Slices were subsequently transferred to a submerged chamber containing 'recording solution' maintained at 34–36°C. Whole-cell recordings were obtained from visually identified hippocampal CA1 pyramidal neurons under a water-immersed X40 objective of an Olympus BX51WI microscope. Pipettes had resistances of 5–8 $\text{M}\Omega$. For current-clamp recordings, the internal pipette solution containing (in mM): 118 KMeSO_4 , 15 KCl, 10 HEPES, 2 MgCl_2 , 0.2 EGTA, and 4 Na_2ATP , 0.3 Tris-GTP, 14 Tris-phosphocreatinine (290–300 mOsm, pH 7.3 with KOH). Hippocampal CA1 pyramidal neurons were patched at a holding potential of -70 mV. Series resistance was in the order of 10–20 $\text{M}\Omega$, which was compensated by 60%–80% during the experiments. Recordings were discarded if the series resistance increased by more than 20% during the course of the recordings. Electrophysiological recordings were made using a Multiclamp 700B amplifier (Molecular Devices, Sunnyvale, CA, USA). Recordings were sampled at 10 kHz. Data were acquired and analysed using pCLAMP 10.6 (Molecular Devices, San Jose, CA, USA). AP and AHP indicators were analysed using Clampfit 10.7 (Molecular Devices).

The stimulus protocol (300 pA, 400 ms or 2000 pA, 2 ms, 100 Hz, 20 APs) was used to evoke AHP. AHP were measured as the area under baseline after the stimulus protocol. Amplitude of the mAHP was defined as the minimum voltage level within 200 ms after the stimulus protocol. Amplitude of the sAHP was measured as the voltage level 200 ms after the stimulus protocol (King et al., 2015). Standard exponential function was fit to estimate time constants (τ).

For observing the morphology of hippocampal CA1 pyramidal neurons, recorded neurons were filled with 0.2%(w/v) neurobiotin. Then, the slices containing the fixed neurons cross-linked with 4% paraformaldehyde and stained with streptavidin Alexa Fluor 488 or 467 conjugate. Fluorescent images were obtained using a confocal microscope (ZEISS LSM 800) and imported into ImageJ (NIH) for further analysis.

2.12 | Adeno-associated virus construction and injection

The adeno-associated viruses (AAVs) and the negative GFP control were from Shanghai GeneChem. Co., Ltd. The full-length SlackG269S sequence (1–1238 aa) was ligated into modified CV232 (CAG-MCS-HA-Poly A) adeno-associated viral vector. The negative control were ligated into GV634 (CAG-MCS-3 \times Flag-T2A-EGFP-SV40-Poly A) adeno-associated viral vector. The viruses ($>10^{11}$ TU. ml^{-1}) were used in this study. For CA1 viral injection, C57BL/6N mice aged 3 weeks were anaesthetised with isoflurane and placed in a stereotaxic apparatus (RWD Life Science, Sugar Land, TX, USA). Using a 10- μl micro syringe (Hamilton) with a 30-gauge needle (RWD Life Science), 600 nl of the viruses was delivered at 10 $\text{nl}\cdot\text{s}^{-1}$ by a micro-syringe pump

(RWD Life Science) at the following site in each of the bilateral CA1 regions, using the stereotaxic coordinates: -2.5 mm (anterior–posterior) from bregma, ± 2 mm (medio-lateral), -1.5 mm (dorsal–ventral) (Yuan et al., 2024). The syringe was left in place for 5 min after each injection and withdrawn slowly. The exposed skin was closed by surgical sutures and returned to home cage for recovery. All the experiments were conducted after at least 3 weeks of recovery. All the mice were sacrificed after experiments to confirm the injection sites and the viral trans-infection effects by checking EGFP under a fluorescence microscope (ZEISS LSM 510 META NLO).

2.13 | Immunostaining

After deep anaesthesia with sodium pentobarbital, mice were killed by perfusion with 0.5% paraformaldehyde and 0.5% sucrose (wt/vol) in 0.1 M phosphate buffer (pH 7.4). The brain was removed and post-fixed in the same fixative for 24 h, and subsequently immersed in 30% sucrose in 0.1 M phosphate buffer for 48 hr. Cryostat coronal sections (20 μm) were obtained using a freezing microtome (Leica). The sections were rinsed in 0.01 M phosphate-buffered saline (PBS, pH 7.4), permeabilized in 0.5% Triton X-100 in PBS for 30 min, and incubated in a blocking solution (5% BSA, 0.1% Triton X-100 in PBS, vol/vol) at 20–25°C for 2 hr, followed by overnight incubation at 4°C with HA (1:2000, Abbkine, ABT2040) in blocking solution. After a complete wash in PBS, the sections were incubated in Alexa 647-conjugated donkey anti-mouse IgG in blocking solution at 20–25°C for 3.5 h at 20–25°C. The sections were subsequently washed and rinsed in DAPI solution. Images were taken in the linear range of the photomultiplier with a laser scanning confocal microscope (ZEISS LSM 510 META NLO).

2.14 | Kainic acid-induced status epilepticus

Kainic acid was injected i.p. to produce class V seizures. The dose of kainic acid used was 20 $\text{mg}\cdot\text{kg}^{-1}$ for mice (aged 6–8 weeks). Vehicle or carvedilol was administered intragastrically 1 h prior to the intraperitoneal injection of kainic acid. To assess epilepsy susceptibility, seizures were rated using a modified Racine scale: (1) immobility followed by facial clonus; (2) masticatory movements and head nodding; (3) continuous body tremor or wet-dog shakes; (4) unilateral or bilateral forelimb clonus; (5) rearing and falling. Status epilepticus was terminated 1 h after onset with the use of sodium pentobarbital (30 $\text{mg}\cdot\text{kg}^{-1}$). Control groups were treated with sodium pentobarbital only (30 $\text{mg}\cdot\text{kg}^{-1}$).

2.15 | Data and statistical analysis

All experiments and analysis of data were performed in a blinded manner by investigators who were unaware of the genotype or manipulation. For in vitro experiments, the cells were evenly

suspended and then randomly distributed in each well tested. For in vivo experiments, the animals were randomly distributed into various treatment groups. Statistical analyses were performed using GraphPad Prism 9 (GraphPad Software, La Jolla, CA, USA). All data are presented as mean \pm SEM. Before statistical analysis, variation within each group of data and the assumptions of the tests were checked. Comparisons between two independent groups were made using unpaired Student's two-tailed *t* test. Comparisons among non-linear fitted values were made using extra sum-of-squares *F* test. Comparisons among three or more groups were made using one- or two-way analysis of variance followed by Bonferroni's post hoc test. * *P* < 0.05 was taken to show significant differences between group means.

2.16 | Materials

Commercial antibodies used were anti-Slack (Cat# ab94578, [RRID: AB_10674494](#); Abcam, Cambridge, UK), anti-HA Tag Mouse Monoclonal Antibody (Cat# A02040; Abbkine, Wuhan, China), anti- β -actin Mouse Monoclonal Antibody (Cat# B1029; Biodragon, Suzhou, China), anti-Na, K-ATPase α 1 Rabbit Polyclonal Antibody (Abbkine, Cat# ABL1141), HRP goat anti-mouse IgG LCS (Biodragon, Cat# BF03001), HRP mouse anti-rabbit IgG LCS (Abbkine, Cat# A25022) and Alexa Fluor 647 donkey anti-mouse IgG (Thermo Fisher Scientific, Cat# A-31571, [RRID: AB_162542](#)). GPCR Extraction Reagent was from Thermo Fisher Scientific; NP40 lysis buffer was from Beyotime, protease inhibitor mixture cocktail was from Roche Applied Science (Basel, Switzerland), rabbit IgG and mouse IgG were from Santa Cruz (Dallas, TX, USA) and Protein G Dynabeads were from Invitrogen (Carlsbad, CA, USA). Kainic acid, sodium pentobarbital, quinidine, sodium valproate, levetiracetam and carbamazepine were supplied by Sigma Aldrich. Carvedilol, dronedarone and thioridazine were supplied by Meilunbio (Dalian, China); chlorpromazine was from Energy Chemical (Jiaying, China); propafenone was from Aladdin (Beijing, China).

2.17 | Nomenclature of targets and ligands

Key protein targets and ligands in this article are hyperlinked to corresponding entries in <https://www.guidetopharmacology.org> and are permanently archived in the Concise Guide to PHARMACOLOGY 2023/24 (Alexander, Christopoulos et al., 2023; Alexander, Mathie et al., 2023).

3 | RESULT

3.1 | Patient history

Here, we report a Chinese girl with EIMFS who presented an intractable seizure disorder and a severe developmental delay. The focal

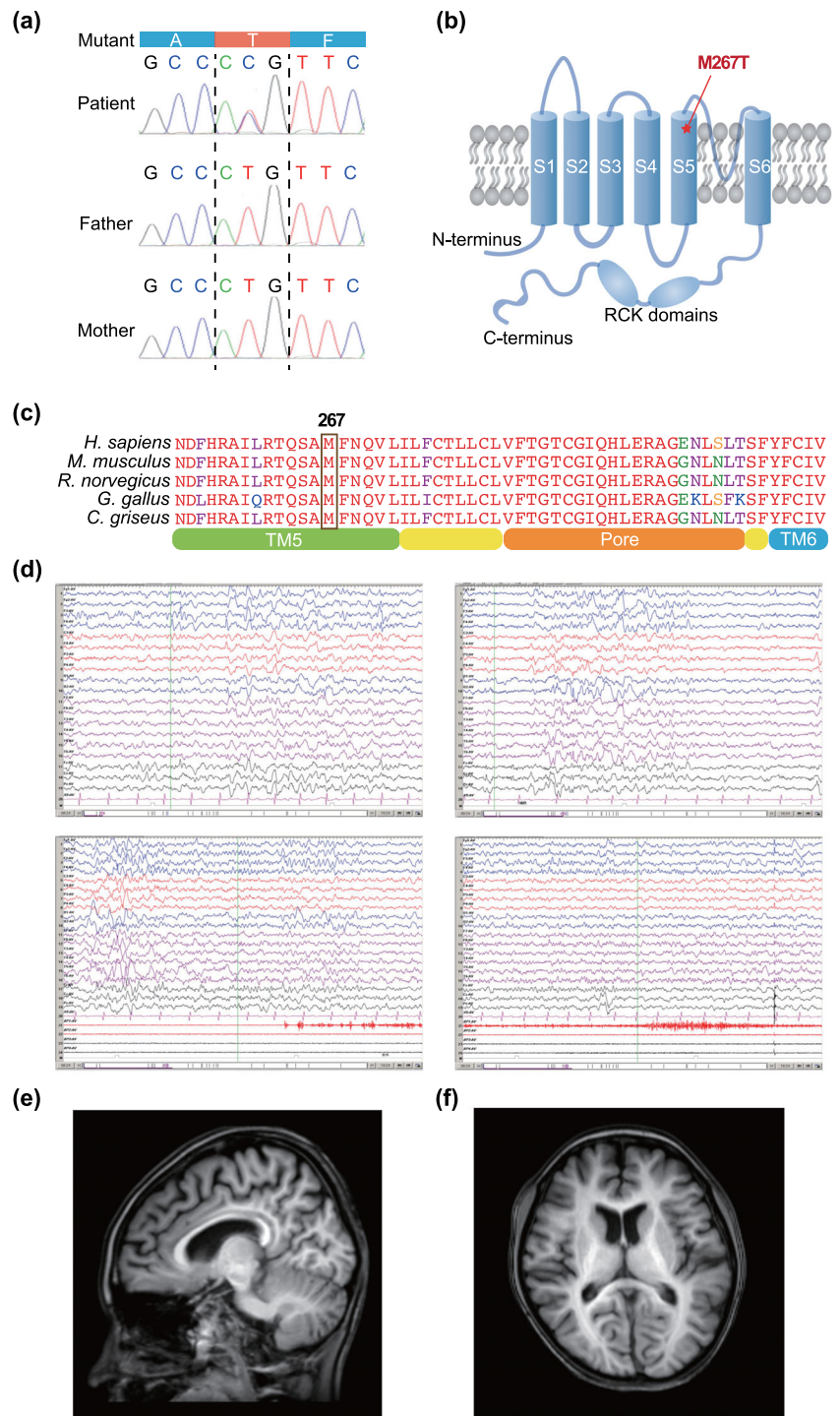
seizures started when the patient was 4 months old and worsened by the eighth month. At 1 year of age, frequent generalized tonic-clonic seizures occurred, development regressed and microcephaly was identified in the patient.

Whole exome sequencing (WES) revealed a heterozygous de novo *KCNT1* mutation (NM_020822: c.800 T > C, p. Met267Thr) (Figure 1a), which has been previously reported in a patient with autosomal dominant nocturnal frontal lobe epilepsy (ADNFLE) without clinical or functional characterization (Meng et al., 2017). The p.M267 is located in the S5 segment near the pore domain and is highly conserved across different species (Figure 1b,c). In silico prediction tools (such as PolyPhen2, SIFT and Mutation Taster) suggested the p.M267T mutation to be disease-causing (Table S2).

The video-electroencephalograph (EEG) revealed the occurrence of frequent seizures during sleep based on blinking, squatting and irregular movements of the limbs. The EEG showed that mainly diffused slow waves in θ rhythm were observed in the background (Figure 1d, up left) and multifocal discharges originating from the right anterior and posterior head regions in the interictal phase (Figure 1d, up right). During the ictal phase, low amplitude fast activity at a frequency of 20 Hz originated from the right frontal and anterior temporal regions (Figure 1d, down left). The increasing amplitude and reducing frequency of the spikes indicated the spread of the seizures to the right hemisphere. The slow wave was gradually inserted and became a diffuse slow wave, lasting for approximately 2 min (Figure 1d, down right). These clinical and EEG features confirmed the diagnoses of EIMFS. The MRI images revealed that the sulci are widened and there is shrinkage of gyri, indicating mild brain atrophy (Figure 1e,f).

The following antiepileptic medications were administered to the patient: [levetiracetam](#), [oxcarbazepine](#), [topiramate](#), [phenobarbital](#), [lamotrigine](#), [valproate](#), [clonazepam](#), vitamin B6 and [quinidine](#). Briefly, the valproate therapy was initiated after the second seizure episode when the patient was 8 months old. Next, topiramate was introduced to the treatment regimen when the seizure frequency of the patient increased at the age of 1 year; however, it was unable to effectively lower the seizure frequency. Subsequently, phenobarbital was introduced, which led to a marked improvement in seizure control, resulting in a notable 6-month seizure-free interval. The seizure frequency of the patient increased at 4 years of age, following which, the patient was treated with a combination of antiepileptic drugs, including 50-mg.day⁻¹ topiramate, 75-mg.day⁻¹ phenobarbital and 500-mg.day⁻¹ levetiracetam. However, this combination therapy could not effectively control the epileptic episodes of the patient. At the age of 7 years, the medication regimen comprised 720-mg.day⁻¹ valproate and 87.5-mg.day⁻¹ lamotrigine; however, the patient continued to experience three to four seizure episodes per day. When the patient was 10 years old, quinidine was administered, which showed some anti-seizure efficacy. However, owing to severe side effects including anorexia, excessive weight loss, weakness and sitting instability, quinidine treatment was discontinued.

FIGURE 1 Patient clinical information and genetic analysis. (a) Sanger sequencing demonstrating de novo KCNT1 variant (NM_020822.3, c [800T > C]; p[Met267Thr]. (b) Diagram showing the KCNT1 protein structure and the position of M267T mutation. (c) The alignment of KCNT1 orthologous peptide sequences with box highlighting the amino acid influenced by the nucleotide mutation of 800T > C. (d) Representative EEG recordings of the patient in interictal and ictal phase. Up left: interictal multifocal epileptic discharges. Up right: diffused slow waves. Down left and down right: focal seizure with ictal discharges. (e,f) MRI images of the patient. Panel (e) shows the sagittal plane of MRI image of the patient's brain. Panel (f) shows the transverse plane of MRI image of the patient's brain.



3.2 | The KCNT1 M267T mutation generated a GOF channel phenotype

To evaluate the effect of the M267T mutation on Slack channel properties, we performed two-electrode voltage-clamp recordings in *X. laevis* oocytes expressing wild-type (WT) or mutant human KCNT1 constructs. Notably, the currents generated by WT and M267T Slack channels were similar in terms of voltage dependence and kinetic behaviour (Figures 2a–c and S1). The current amplitude was

quantified at a potential of +10 mV to avoid potential bias in the results because of amplifier saturation at higher depolarizing potentials. The M267T Slack channel-produced currents presented three-fold greater amplitudes than those by WT channels (Figure 2d). Furthermore, the analysis of activation kinetics revealed that M267T channels activated faster than WT channels (Figure 2e).

To determine whether the GOF channel phenotype of M267T Slack channels resulted from facilitated Slack protein membrane-expression, we performed a surface biotinylation assay in HEK293T

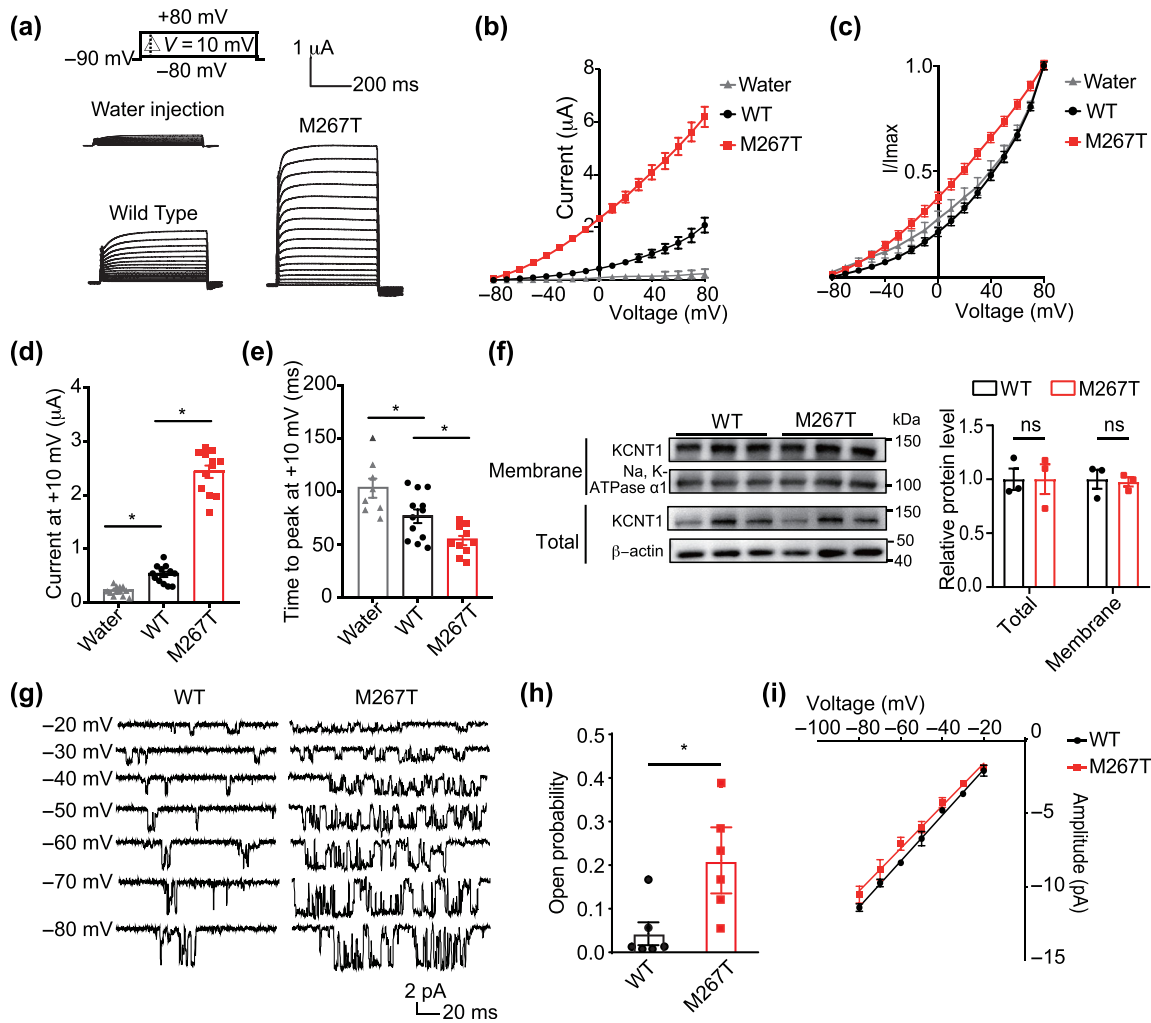


FIGURE 2 M267T mutation resulted in a gain-of-function channel phenotype. (a) Representative current traces evoked by stepping from -80 to $+80$ mV in 10 -mV increments in oocytes expressing WT or M267T human KCNT1 and control oocytes injected with water. Scale bars apply to all traces. (b) Averaged current–voltage relationship (\pm SEM) for oocytes expressing WT, M267T and control oocytes injected with water ($n = 5, 5$ and 5 , respectively). (c) Averaged and normalized current–voltage relationships for WT, M267T and control oocytes injected with water. Currents were normalized to the value at a test potential at $+80$ mV (I_{max}). (d) Current amplitudes at $+10$ mV for the three groups of oocytes in (b). (e) Activation kinetics shown as mean time to peak current at $+10$ mV for the three groups of oocytes in (b). $*P < 0.05$, significantly different as indicated; unpaired two-tailed Student's t test. Data are presented as means \pm SEM. (f) The total level and plasma membrane expression of KCNT1 WT and M267T. Left: Immunoblot analysis of cell surface biotinylation performed in HEK293T cells expressing KCNT1 WT or M267T. Right: Quantification of KCNT1 total expression and surface expression. $n = 3$, two-way ANOVA with Bonferroni's multiple-comparisons test. (g) Representative single channel records from WT or M267T Slack channels. (h) Histograms depict channel open probabilities for WT and M267T slack channels. $*P < 0.05$, significantly different as indicated; unpaired two-tailed Student's t test. Data are presented as means \pm SEM. (i) Current versus voltage relationships for WT and M267T Slack channels.

cells expressing WT or M267T Slack channels. No significant differences were observed in the total or plasma membrane expression level between WT and M267T Slack channels (Figure 2f).

To investigate whether M267T mutation affected the single-channel properties of Slack channel, we recorded excised inside-out patches from HEK293T cells expressing WT or M267T Slack channels. The open probability (P_o) of M267T Slack channels at a holding potential of -40 mV was approximately five-fold higher than the P_o of WT Slack channels, with no change in single-channel amplitude (Figure 2g–i). The single-channel conductance of M267T Slack channels was similar to that of WT Slack channels (Figure 2i).

These results suggest that the M267T mutation increases the Slack macroscopic current by increasing single-channel open probability.

3.3 | Effects of antiepileptic drugs on M267T slack currents

Several ASMs have been used to suppress seizures in the patient with Slack^{M267T} channels. Among them, quinidine has exhibited the most effective anticonvulsant activity, and sodium valproate and

phenobarbital can moderately reduce seizures. Other ASMs, such as levetiracetam and oxcarbazepine, do not exhibit any notable antiepileptic activity. To assess the parallelism of drug efficacy in clinical and in vitro experiments, four representative drugs used by the patient were selected and tested for their ability to inhibit the Slack currents in vitro. To achieve this, we injected *X. laevis* oocytes with WT or M267T *KCNT1* constructs and performed electrophysiological analyses. Consistent with the clinical results, quinidine markedly inhibited Slack^{M267T} currents; washing of the drug reversed the inhibition activity (Figures 3a–c and S2). Moreover, quinidine extended the time to peak current of Slack^{M267T} channels (Figure S2). The amplitude or time to peak current of the Slack^{M267T} channels was not affected by levetiracetam, sodium valproate, and carbamazepine (Figures 3a–c and S2). These results indicate the consistency of the in vitro results with that of the clinically observed efficacy.

3.4 | Carvedilol inhibited Slack currents

To identify an effective Slack channel inhibitor, we screened 16 FDA-approved compounds (Table S3). These compounds can

block various potassium channels and other types of voltage-dependent ion channels, in cardiomyocytes, neurons and other cell types (Aréchiga et al., 2008; Champéroux et al., 2022; Cheng et al., 2019; Cioclu et al., 2023; Dong et al., 2006; Dopp et al., 2008; Du et al., 2020; Gomma et al., 2001; Patel et al., 2009; Wulff et al., 2009; J. F. Yang et al., 2018). We examined the effects of these drugs on Slack channels expressed in *Xenopus* oocytes with electrophysiological recordings. Notably, 100 μ M carvedilol significantly inhibited both WT and M267T Slack currents, whereas chlorpromazine, propafenone, dronedarone and thioridazine exhibited a weaker inhibition; other drugs had no effect on M267T Slack currents (Figures 4a–c and S3). Additionally, the IC₅₀ values of carvedilol, chlorpromazine, propafenone, dronedarone and thioridazine on Slack currents in the HEK293T cells revealed that the IC₅₀ value of carvedilol was the lowest (Figure 4d). Inhibition of Slack currents was concentration-dependent and was quantified by fitting the dose–response curve with a Hill equation. Altogether, these results suggested that carvedilol was a potent inhibitor of the Slack channels.

We also assessed the effect of carvedilol on two previously reported *KCNT1* mutants, R428Q (Barcia et al., 2012; Bearden

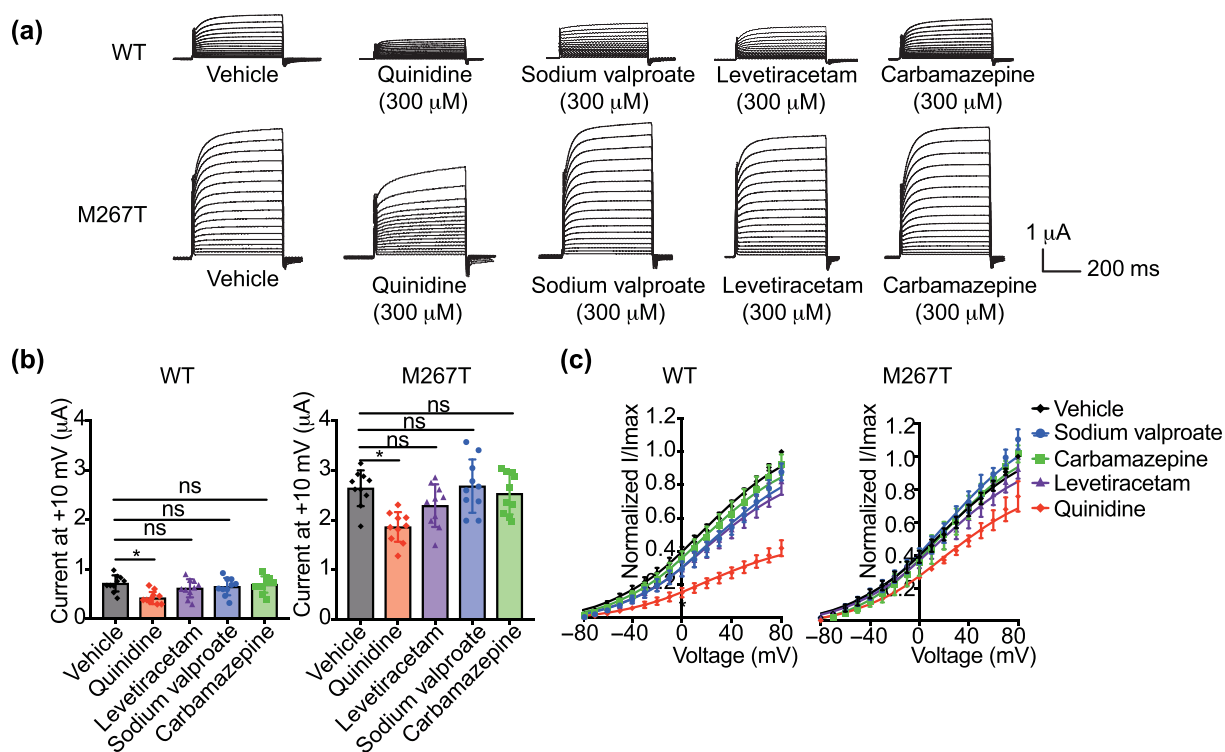


FIGURE 3 Effects of anti-epilepsy drugs on Slack currents. (a) Representative current traces obtained from oocytes expressing wild-type, M267T channels in vehicle control and in the presence of 300- μ M quinidine, 300- μ M sodium valproate, 300- μ M levetiracetam and 300- μ M carbamazepine. Scale bars apply to all traces. Oocytes were held at -90 mV and evoked by stepping from -80 to $+80$ mV in 10-mV increments. (b) Comparison of average current amplitude derived from measurements made at $+10$ mV for WT and M267T mutant channels in vehicle control and in the presence of 300- μ M quinidine, 300- μ M sodium valproate, 300- μ M levetiracetam and 300- μ M carbamazepine. Data are presented as means \pm SEM; WT, $n = 5$; M267T, $n = 5$; $P < 0.05$, significantly different as indicated; ns, not significant; unpaired two-tailed Student's t test. (c) Normalized average current–voltage relationships for WT and M267T channels in the presence of vehicle, 300- μ M quinidine, 300- μ M sodium valproate, 300- μ M levetiracetam and 300- μ M carbamazepine (WT, $n = 5$; M267T, $n = 5$). Currents were normalized to the value before the application of drugs at a test potential of $+80$ mV (I_{max}).

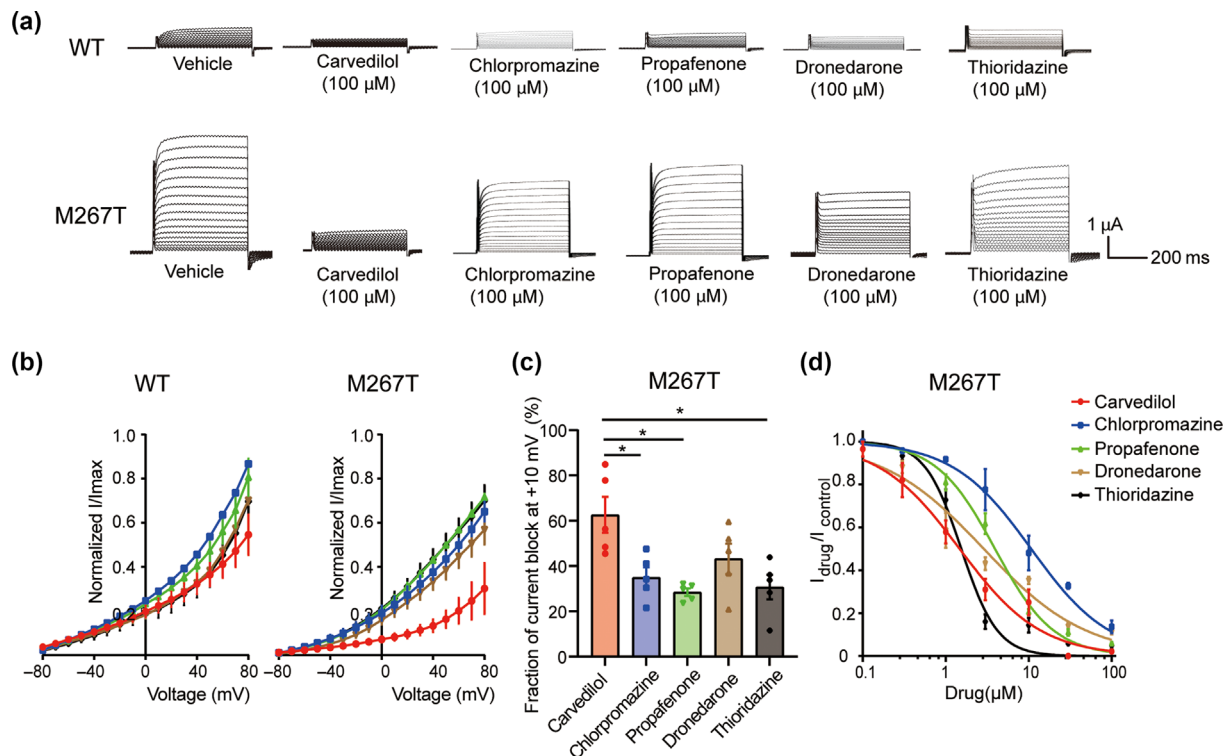


FIGURE 4 FDA-approved drugs inhibited M267T Slack currents. (a) Representative current traces obtained from oocytes expressing wild-type, M267T channels in vehicle control and in the presence of 100-µM carvedilol, 100 µM chlorpromazine, 100-µM propafenone, 100-µM dronedarone and 100-µM thioridazine. Scale bars apply to all traces. Oocytes were held at -90 mV and evoked by stepping from -80 to +80 mV in 10-mV increments. Normalized average current-voltage relationships for WT and M267T Slack channels (b) in the presence of 100-µM carvedilol, 100-µM chlorpromazine, 100-µM propafenone, 100-µM dronedarone and 100-µM thioridazine. $n = 5, 5, 5, 5$ and 5 , respectively. Currents were normalized to the value before the application of drugs at a test potential of +80 mV (I_{max}). Data shown are means \pm SEM. (c) Fraction of current block at +10 mV for Slack^{M267T} illustrating the degree of block by 100-µM carvedilol, 100-µM chlorpromazine, 100-µM propafenone, 100-µM dronedarone and 100-µM thioridazine. Data are presented as means \pm SEM; $n = 5$ for each group. * $P < 0.05$, significantly different as indicated; paired two-tailed Student's t test. (d) IC_{50} of carvedilol, chlorpromazine, propafenone, dronedarone and thioridazine on M267T Slack currents in the HEK293T cell line. (carvedilol, $IC_{50} = 1.47 \mu M$, $n = 7$; chlorpromazine, $IC_{50} = 10.69 \mu M$, $n = 7$; propafenone, $IC_{50} = 3.92 \mu M$, $n = 7$; dronedarone, $IC_{50} = 2.87 \mu M$, $n = 10$; thioridazine, $IC_{50} = 1.54 \mu M$, $n = 8$). Data are shown as mean \pm SEM and are fitted to dose-response curve with a Hill equation.

et al., 2014; Møller et al., 2015; Ohba et al., 2015) and G288S (Ishii et al., 2013; Kim et al., 2014; Møller et al., 2015; Ohba et al., 2015). Notably, 300 µM carvedilol significantly inhibited R428Q and G288S Slack currents (Figure 5a-c) with different inhibitory efficiencies (Figure 5e). Additionally, carvedilol prolonged the time to peak current of the WT and mutant Slack channels (Figure 5d). The IC_{50} values of carvedilol and quinidine on the Slack currents in HEK293T cells revealed the higher potency of carvedilol, compared with that of quinidine (Figure 5f). Notably, quinidine exhibited notable potency in inhibiting M267T Slack currents than inhibiting WT Slack currents (Figure 5g).

To investigate the mechanism by which carvedilol inhibited Slack channels, we carried out single-channel recordings in inside-out patches. Bath-application of 10-µM carvedilol markedly reduced the single-channel P_o of M267T Slack channels without affecting the amplitude (Figure 5h-j). These results suggest that carvedilol can directly inhibit the Slack channels by reducing the single-channel open probability.

3.5 | The M267T Slack channels increased the excitability of hippocampal CA1 pyramidal neurons

To investigate the role of Slack^{M267T} in eliciting neuronal excitability, we performed in utero electroporation (IUE) to express Slack^{WT} and Slack^{M267T} in the mouse hippocampal CA1 pyramidal neurons. E14.5 embryos were electroporated with WT or M267T *KCNT1* plasmids. After postnatal 6 weeks, acute brain slices were prepared, and whole-cell current-clamp recording was performed on CA1 pyramidal neurons that exhibited green fluorescence, indicating exogenous Slack channel expression (Figure 6a,b). When membrane potentials were held at -70 mV with current injection, neurons carrying M267T Slack channels generated significantly greater numbers of action potentials (APs) than those expressing WT Slack channels (Figure 6c,d).

The Slack channels can contribute to sAHP (Franceschetti et al., 2003; Schwandt et al., 1989). Hence, the effects of M267T Slack mutations on the AP frequency in the first 200 ms and the last 200 ms of a 400-ms step were investigated. Notably, the spike

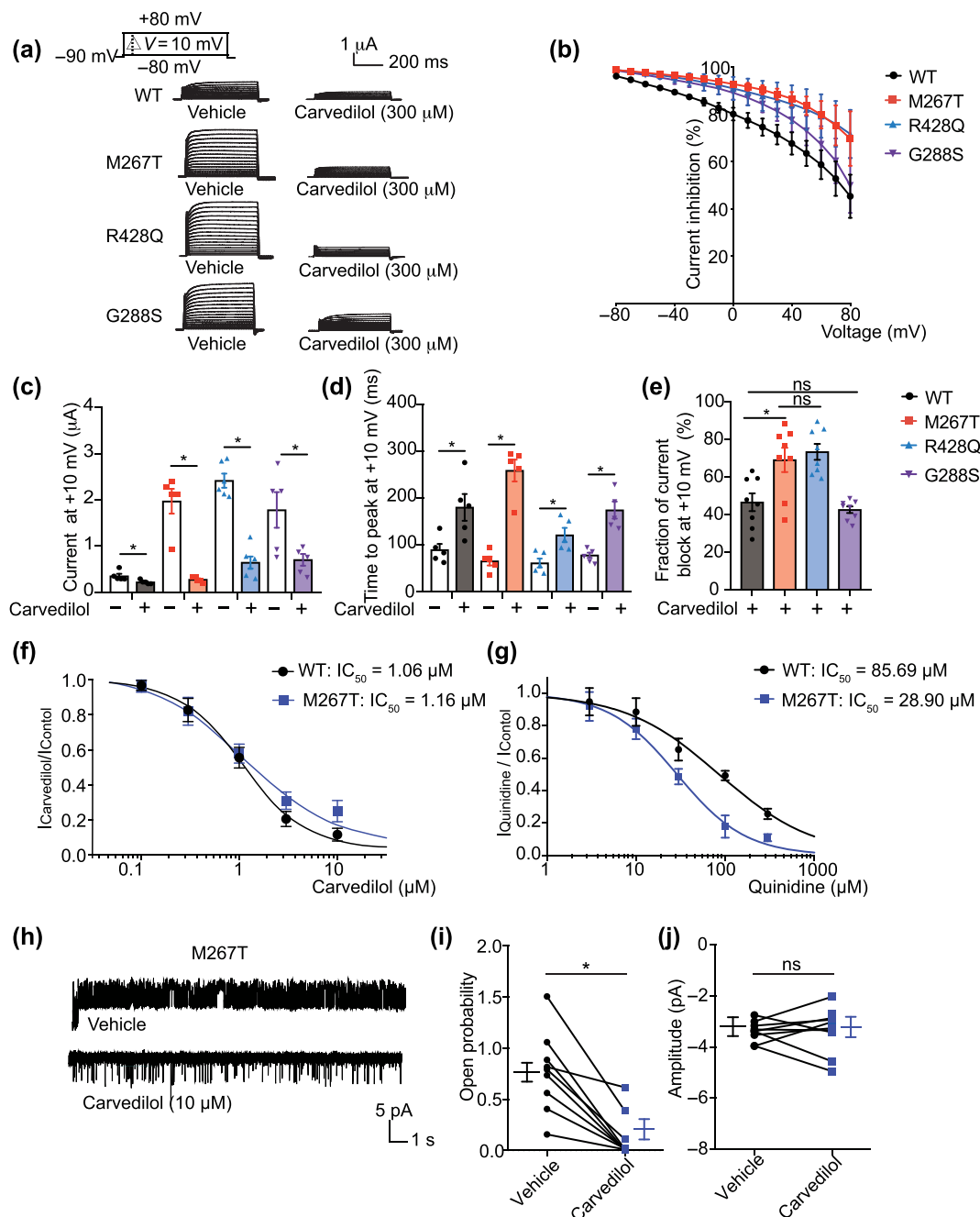


FIGURE 5 Carvedilol inhibited wild type and mutant Slack currents. (a) Representative current traces obtained from oocytes expressing wild-type, M267T, R428Q, G288S Slack in vehicle control and in the presence of 300- μM carvedilol. Scale bars apply to all traces. Oocytes were held at -90 mV and evoked by stepping from -80 to $+80$ mV in 10-mV increments. Percentage of current inhibition (b), current at $+10$ mV (c), time to peak current at $+10$ mV (d), fraction of current block at $+10$ mV (e) for WT and mutant Slack channels in the presence of 300- μM carvedilol (WT, $n = 6$; M267T, $n = 6$; R428Q, $n = 5$; G288S, $n = 5$). Currents were normalized to the value before the application of carvedilol at a test potential of $+80$ mV (I_{max}). Data are presented as means \pm SEM. $*P < 0.05$, significantly different as indicated; ns, not significant; unpaired two-tailed Student's t test. IC_{50} of carvedilol (f) and quinidine (g) on WT and M267T Slack currents in the HEK293T cell line. $n = 5$, 5, respectively. Data are shown as mean \pm SEM and are fitted to dose-response curve with a Hill equation. Significance of fitted IC_{50} values compared to WT was analysed using extra sum-of-squares F test. (h) Representative single channel records from M267T Slack channels with vehicle or 10- μM carvedilol perfusion. Histograms depict channel open probabilities (i) and amplitude (j) for M267T slack channels with vehicle or 10 μM carvedilol perfusion. Data are presented as means \pm SEM. $P < 0.05$, significantly different as indicated; ns, not significant; paired two-tailed Student's t -test.

frequency, and thus, the interspike interval in the first 200 ms were not considerably affected (Figure 6e). The firing frequency in the last 200 ms was significantly increased (Figure 6f). The effects of M267T

Slack mutations on mAHP and sAHP following a 400 ms of 300 pA current injection (Figure 6g) were as follows: the mAHP amplitude was considerably reduced (Figure 6h) and the time to peak mAHP was

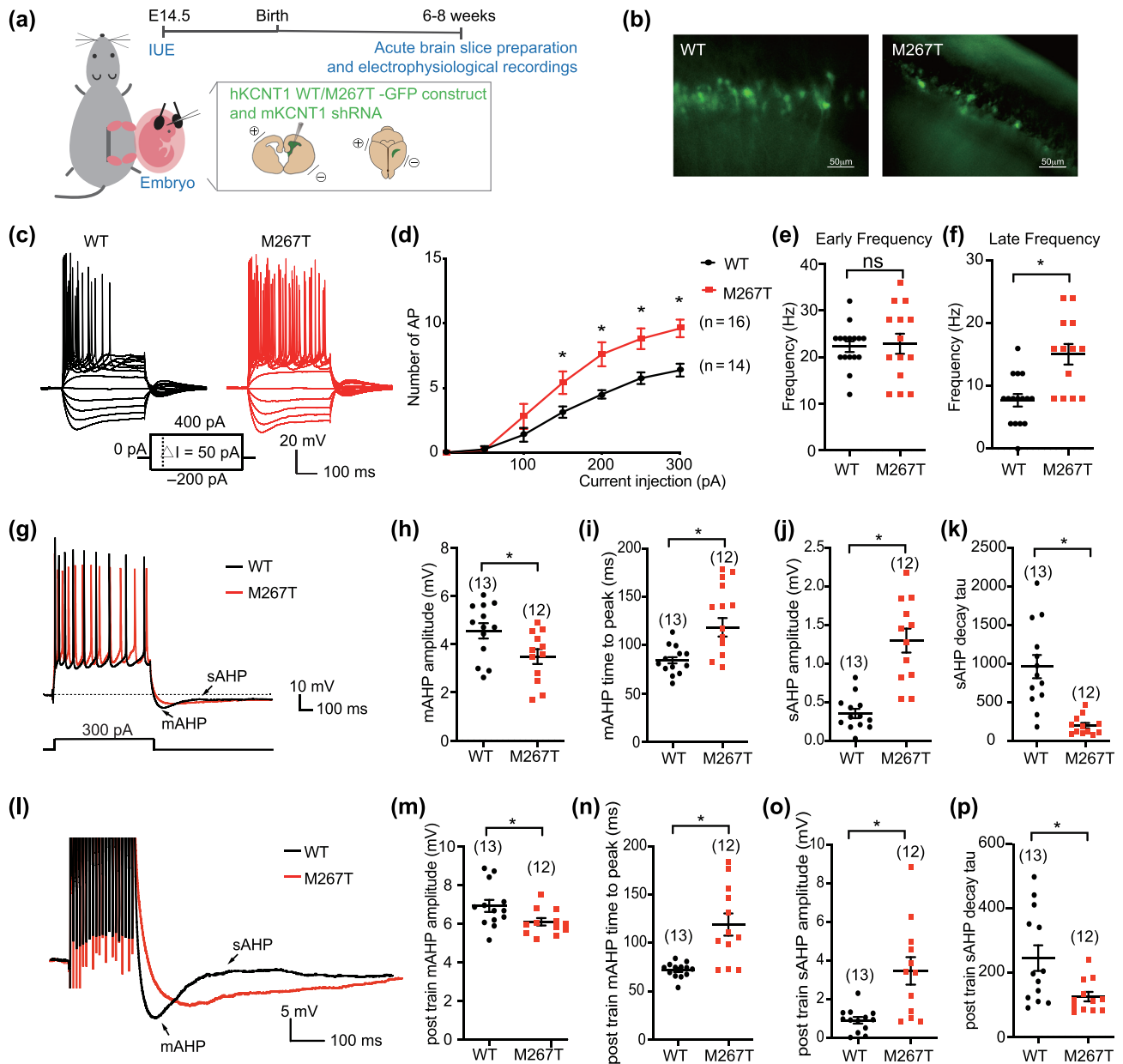


FIGURE 6 The M267T Slack channels increased excitability of neurons in hippocampal CA1. (a) Schematic illustration depicting in utero injection and electroporation of Wild type or M267T KCNT1-GFP constructs into the ventricle of E14.5 embryonic mouse brain. Brain slices were prepared from postnatal 6 to 8 weeks mice. Whole-cell current-clamp recordings were performed on CA1 pyramidal neurons with green fluorescence. (b) Example images of brain slices from postnatal pups taken from E14.5 in utero electroporated pregnant mouse injected with Wild type or M267T KCNT1-GFP construct. Scale bar = 50 μ m. (c) Representative traces obtained from CA1 neurons from WT and M267T Slack mice in response to a series of 400-ms current stepping from -200 to +400 pA with increments of 50 pA. For comparison reasons, the recordings were obtained at the fixed potential of -70 mV. (d) Graphs demonstrate average numbers of action potentials obtained in response to varying depolarizing current pulses when the soma was held at -70 mV. Spike frequency within the first 200 ms (e) or the last 200 ms (f) of a 400-ms step. Data are presented as means \pm SEM. * P < 0.05, significantly different as indicated; ns, not significant; unpaired two-tailed Student's t test. (g) Representative traces obtained from CA1 neurons in response to 300-pA current injection. For comparison reasons, the recordings were obtained at the fixed potential of -70 mV. mAHP amplitude (h), time to peak mAHP (i), sAHP amplitude (j) and sAHP decay time constant (k) obtained from CA1 neurons with 300-pA current injection. (l) The AHPs were evoked after sequences of 20 APs elicited by injecting brief trains (200 ms) of 100 Hz depolarizing stimuli (post train AHPs). Post train mAHP amplitude (m), time to peak post train mAHP (n), post train sAHP amplitude (o) and post train sAHP decay time constant (p) as showed in (l). Data are presented as means \pm SEM. * P < 0.05, significantly different as indicated; unpaired two-tailed Student's t test.

prolonged (Figure 6i); the sAHP amplitude was increased (Figure 6j) and the sAHP decay time constant (τ) was reduced (Figure 6k). We further performed current-clamp recordings with minimal positive

current injection to induce single AP in the hippocampal CA1 neurons. Notably, M267T Slack channels did not affect the intrinsic membrane properties of single AP in neurons (Table S4). Additionally, a train of

20 APs at -70 mV resulted in a fast hyperpolarization (fAHP) followed by a mAHP and a sAHP in all the cells (Figure 6l). The post-train mAHP amplitude was markedly reduced by the M267T Slack channels (Figure 6m and Table S5), and the time to peak of post-train mAHP was prolonged (Figure 6n and Table S5). The post-train sAHP amplitude was increased (Figure 6o) and the post-train sAHP decay time constant was reduced (Figure 6p). These results suggest that the M267T Slack channels can increase the neuronal excitability of hippocampal CA1 pyramidal neurons by modulating the mAHP and sAHP.

3.6 | Carvedilol inhibited the hyperexcitability of the hippocampal CA1 pyramidal neurons carrying M267T Slack channels

We next evaluated the effects of carvedilol on excitability of the hippocampal CA1 pyramidal neurons carrying M267T Slack channels. Application of $10\ \mu\text{M}$ carvedilol significantly reduced the number of APs (Figure 7a,b). The firing frequency for the first 200 ms and the last 200 ms were both decreased (Figure 7c,d). Additionally, carvedilol notably increased the mAHP amplitude (Figure 7f), and reduced the time to peak mAHP (Figure 7g), decreased sAHP amplitude (Figure 7h) and extended the sAHP decay time constant (Figure 7i). Interestingly, carvedilol raised the AP threshold (Figure 7k), decreased AP amplitude (Figure 7l) and increased afterdepolarization (ADP) magnitude (Figure 7m), without affecting the AP half width or time to peak AP (Figure 7n,o).

The assessment of the effects of carvedilol on mAHP and sAHP following a train of 20 APs at -70 mV (Figure 7p) revealed that carvedilol considerably increased the post-train mAHP amplitude (Figure 7q), and reduced the time to peak of post-train mAHP (Figure 6r), decreased post-train sAHP amplitude (Figure 7s) and extended the post-train sAHP decay time constant (Figure 7t). These results suggest that carvedilol can inhibit the neuronal excitability of the hippocampal CA1 pyramidal neurons carrying M267T Slack channels by modulating the properties of AHP and AP.

We also evaluated the effects of carvedilol on excitability of the hippocampal CA1 pyramidal neurons in WT mice. Notably, $10\text{-}\mu\text{M}$ carvedilol markedly reduced the AP number (Figure S4b), raised the AP threshold (Figure S4c), and decreased the AP amplitude (Figure S4d). After the train of 20 APs at -70 mV stimulation (Figure S4e), carvedilol significantly decreased the post-train sAHP amplitude (Figure S4h) but exhibited no effect on mAHP (Figure S4f,g). Moreover, the effects of carvedilol on CA1 pyramidal neurons in juvenile WT mice were consistent with those observed in adult WT mice (Figure S5). These results show that carvedilol can reduce neuronal excitability of the WT hippocampal CA1 pyramidal neurons by modulating the properties of sAHP and AP.

3.7 | Carvedilol suppressed seizure susceptibility

To assess the anticonvulsant activity of carvedilol, we used the model of acute seizures, induced by kainic acid, in mice (Ben-Ari &

Cossart, 2000; Racine, 1972). We injected kainic acid ($20\text{-mg}\cdot\text{kg}^{-1}$, i.p.) into wild-type mice, pretreated with different doses of carvedilol or vehicle, to elicit status epilepticus. Notably, seizure progression was significantly slower in carvedilol-treated mice (Figure 8a). Furthermore, carvedilol markedly increased the latency to the first generalized seizure (Class IV seizure) and reduced maximum seizure severity with that in the vehicle control (Figure 8b,c). These results indicate that carvedilol exhibited anticonvulsant effects in the model of epilepsy induced by kainic acid in mice.

To clarify the anti-seizure effect of carvedilol on mice carrying the KCNT1 mutant, we used the mice carrying the Slack mutant, as established in our lab previously (Yuan et al., 2024). We induced an in vivo epilepsy model by introducing a Slack^{G269S} variant into C57BL/6N mice using adeno-associated virus (AAV) injection to mimic the human Slack mutation G288S. We delivered stereotactic injections of AAV9 containing expression cassettes for Slack^{G269S} (or GFP negative controls) into the hippocampal CA1 region of 3-week-old C57BL/6N mice (Figure 8d,e). At 3- to 5-week intervals after AAV injection, we quantified the seizure susceptibility of mice following the induction by kainic acid ($20\text{-mg}\cdot\text{kg}^{-1}$, i.p.) of temporal lobe epilepsy. Either the vehicle or $50\ \text{mg}\cdot\text{kg}^{-1}$ of carvedilol was administered intragastrically 1 h prior to the i.p. injection of kainic acid. We assessed a time course of kainic acid-induced seizure stages at 5 min intervals and found that viral expression of Slack^{G269S} resulted in faster seizure progression in mice, compared to control GFP expression, and carvedilol slowed down seizure progression of Slack^{G269S} mice (Figure 8f). Slack^{G269S} also significantly reduced the latency to first generalized seizure, and carvedilol increased the latency to first generalized seizure of Slack^{G269S} mice (Figure 8g). The percentage of mice with stage V seizures also increased in Slack^{G269S} mice, and carvedilol effectively decreased the percentage of mice with stage V seizures (Figure 8h). Taken together our results showed that viral expression of Slack^{G269S} significantly increased seizure susceptibility in mice, and that carvedilol effectively reduced the seizure susceptibility of Slack^{G269S} mice.

4 | DISCUSSION

Slack belongs to the high conductance K^+ channel family activated by intracellular Na^+ (namely K_{Na} channels), which is reported to participate in the AHP in cortical neurons, hippocampal CA1 pyramidal neurons and dorsal root ganglion (DRG) neurons (Gao et al., 2008; Liu & Stan Leung, 2004; Shore et al., 2020). For example, the K_{Na} currents contribute to AHP generation and maintenance following the rhythmic burst recurrence during sustained depolarizations in the neocortical intrinsic bursting neurons (Franceschetti et al., 2003). In addition, KCNT1-epilepsy associated mutations also modulate AHP and neuronal excitability. Notably, studies have demonstrated that the Y796H variant increases AHP amplitude and reduces excitability in non-fast-spiking GABAergic neurons in cortical layer 2/3, while exhibiting no effect on fast-spiking GABAergic or glutamatergic neurons (Shore et al., 2020). However, the functional properties and physiological roles of the WT and mutant Slack currents have not been fully

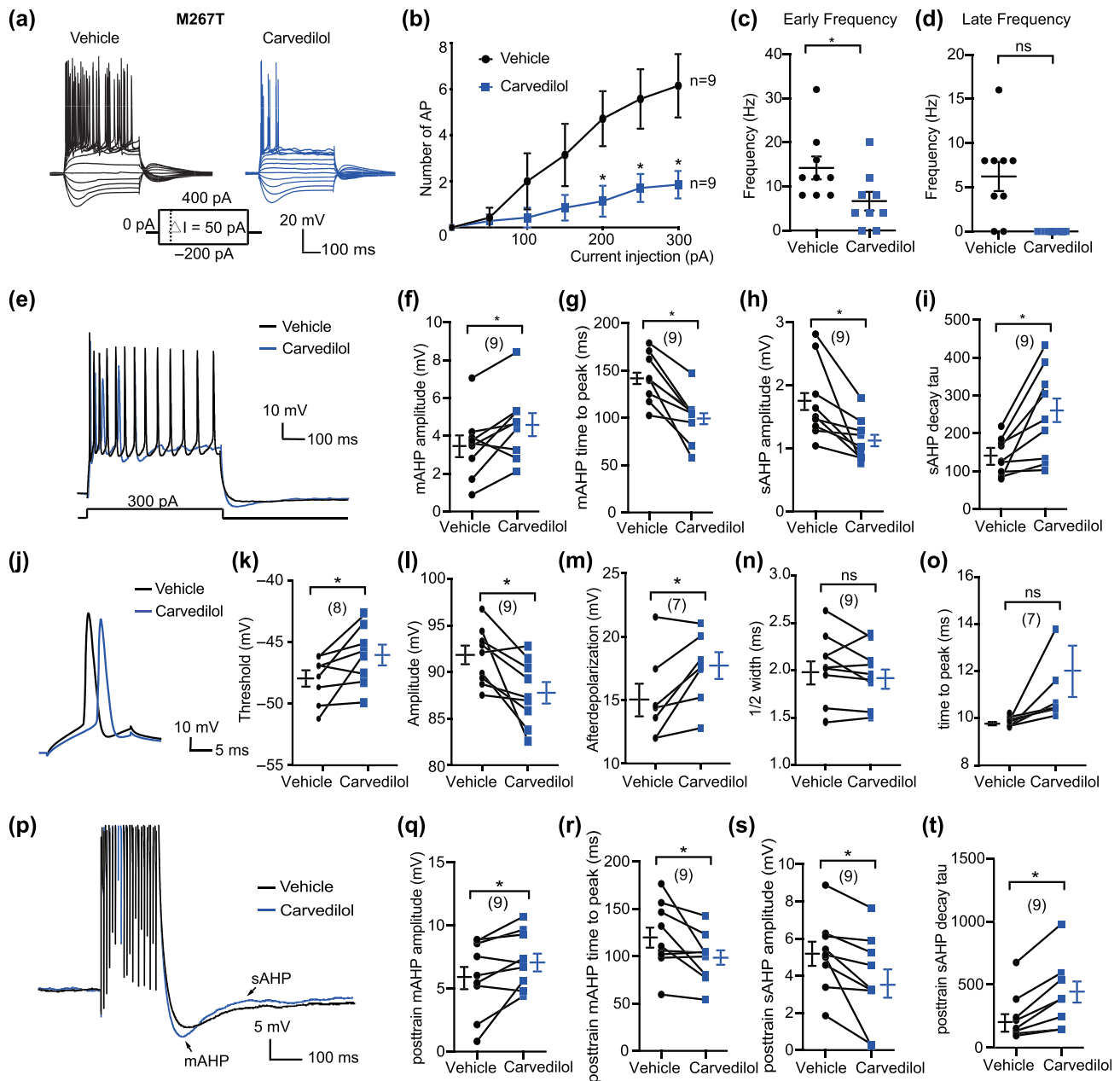


FIGURE 7 Carvedilol reduced excitability of M267T Slack-expressed neurons in hippocampal CA1. (a) Representative traces obtained from M267T Slack-expressed CA1 neurons with vehicle or 10- μ M carvedilol perfusion in response to a series of 400-ms current stepping from -200 to $+400$ pA with increments of 50 pA. For comparison reasons, the recordings were obtained at the fixed potential of -70 mV. (b) Average numbers of action potentials obtained in response to varying depolarizing current pulses when the soma was held at -70 mV. Spike frequency within the first 200 ms (c) or the last 200 ms (d) of a 400-ms step. Data are presented as means \pm SEM. * $P < 0.05$, significantly different from vehicle; unpaired two-tailed Student's t test. (e) Representative traces obtained from CA1 neurons in response to 300-pA current injection. For comparison reasons, the recordings were obtained at the fixed potential of -70 mV. The effects of 10 μ M carvedilol on mAHP amplitude (f), time to peak mAHP (g), sAHP amplitude (h) and sAHP decay time constant (i) obtained from CA1 neurons with 300-pA current injection. Typical spikes (j), spike threshold (k), spike amplitude (l), spike afterdepolarization (m), spike half width (n) and time to peak (o) obtained from CA1 neurons in presence of vehicle or 10- μ M carvedilol. (p) The effects of 10- μ M carvedilol on post train AHPs. The AHPs were evoked after sequences of 20 APs elicited by injecting brief trains (200 ms) of 100-Hz depolarizing stimuli. Post train mAHP amplitude (q), time to peak post train mAHP (r), post train sAHP amplitude (s) and post train sAHP decay time constant (t) as showed in (p). Data are presented as means \pm SEM. * $P < 0.05$, significantly different from vehicle; paired two-tailed Student's t test.

elucidated. The results of this study show that M267T mutation-induced enhanced Slack currents resulted in decreased mAHP amplitude, prolonged time to peak mAHP, increased sAHP amplitude and

reduced the sAHP decay time constant τ , leading to hyperexcitability of the hippocampus CA1 pyramidal neurons. It has been reported that K_{Na} mainly contributed to sAHP. Here we found that the Slack also

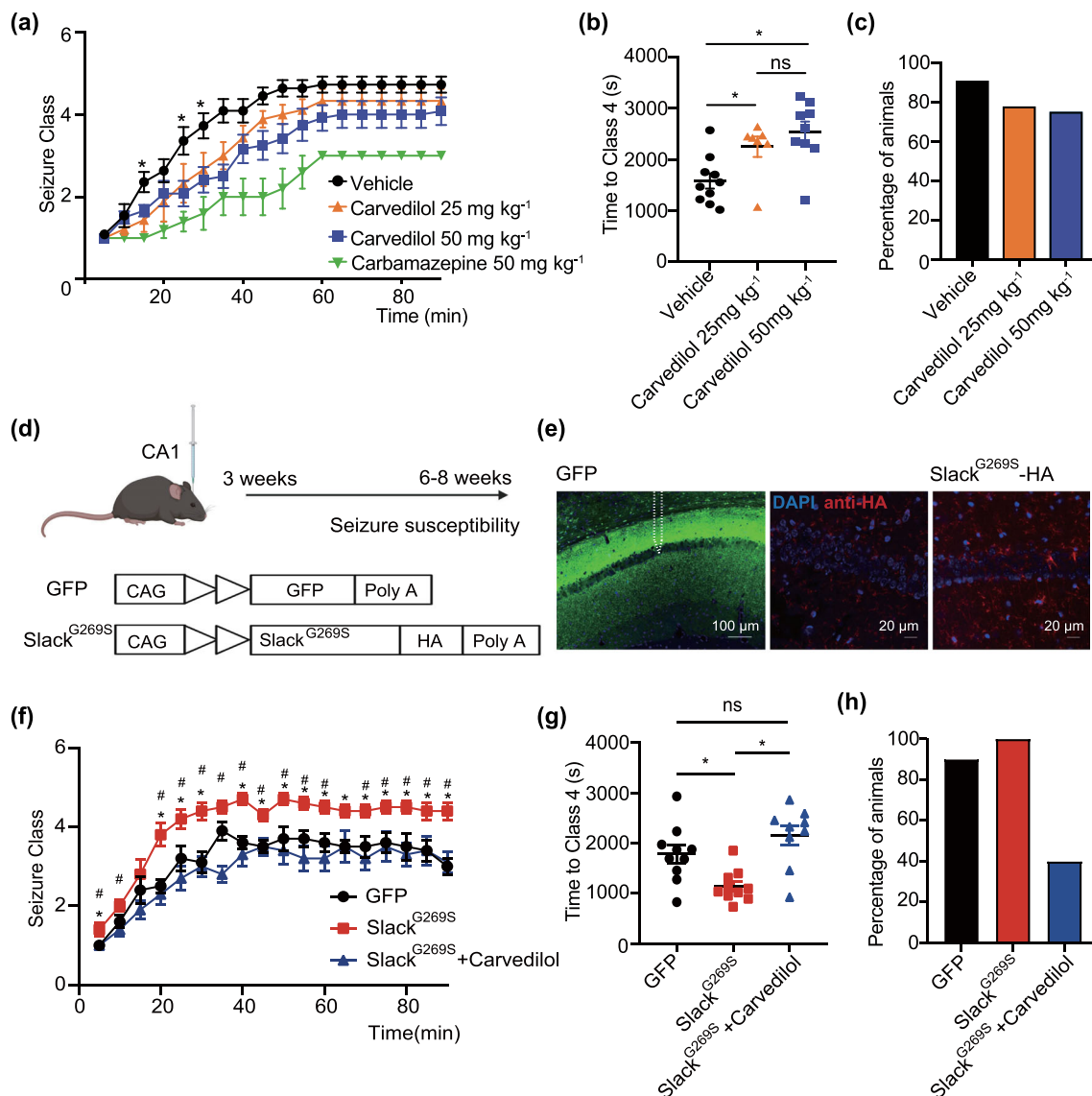


FIGURE 8 Carvedilol suppressed seizure susceptibility of WT and Slack^{G269S} mice. (a) The seizure progression in mice treated with carvedilol or carbamazepine or vehicle. * $P < 0.05$, significantly different from treated mice; unpaired two-tailed Student's t test. (b) The time taken to reach Class 4 seizure after kainic acid (KA) administration from carvedilol and vehicle injected mice. * $P < 0.05$, significantly different as indicated; unpaired two-tailed Student's t test. (c) The incidence of maximum seizure class reached during the course of the experiments in (a). (d) Study design and timeline for the stereotactic injection model, and architecture for expression cassettes of AAVs. (e) Left: GFP expression in hippocampal CA1. Dotted line, the injection location of AAVs. Right: Immunofluorescence of HA-tagged Slack (red) and DAPI (blue) in hippocampal CA1 pyramidal cell layer at 5 weeks after viral injection of Slack^{G269S} into CA1 of mice. The seizure progression (f), the time taken to reach Class 4 seizure after kainic acid administration (g), the incidence of maximum seizure class reached during the course of the experiments (h). * $P < 0.05$, Slack^{G269S} group significantly different from GFP group; # $P < 0.05$, Slack^{G269S} group significantly different from Slack^{G269S}+carvedilol group, unpaired two-tailed Student's t -test.

affects properties of mAHP. We hypothesized that the Slack M267T mutation may influence the expression and function of other voltage-gated channels, such as SK, HCN, and K_v7 channels (Church et al., 2019; Sahu & Turner, 2021). For example, recent results show that the functional and physical interaction between HCN and Slack channels regulates neuronal excitability in mPFC pyramidal neurons (Wu et al., 2024).

Previously, quinidine, an antiarrhythmic drug, has been reported as a potential precision therapy for *KCNT1*-related epilepsy (Bearden

et al., 2014; Milligan et al., 2014). However, the clinical data on the efficacy of quinidine in patients with *KCNT1* mutations is inconsistent (Mullen et al., 2018; Numis et al., 2018). This may be possibly because of the low blood-brain barrier (BBB) permeability of quinidine, and its potential to cause serious side effects, such as prolonged QT interval, arrhythmias, rash, and skin discoloration (Sindrup et al., 1996). These studies indicated the lack of an established treatment, and warranted an urgent clinical need for a more effective and specific drug for *KCNT1*-related epilepsies. In the present work, carvedilol, a drug

commonly used to treat chronic heart failure, left ventricular dysfunction, and hypertension was identified as a potential inhibitor of Slack channels. Carvedilol has been reported to act on β - and α_1 -adrenoceptors, and on sodium, potassium, and calcium channels (Atkin et al., 2018; Cheng et al., 2019; El-Sherif & Turitto, 2005). Increasing evidence indicates the neuroprotective properties of carvedilol. Thus, carvedilol exhibited neuroprotective effects in the cultured rat cerebellar and hippocampal CA1 neurons of gerbils exposed to brain ischemia (Lysko et al., 1992). Additionally, carvedilol could re-establish basal synaptic transmission, enhance neuronal plasticity, and suppress neuronal hyperexcitability in a mouse model of Alzheimer's disease (Arrieta-Cruz et al., 2010). The results of the present study show that carvedilol effectively inhibited the M267T Slack mutation-mediated enhanced neuronal excitability, exhibiting anti-epileptic activity in a mouse epilepsy model. We found that carvedilol reduced the neuronal excitability of CA1 pyramidal neurons by regulating AHP, raising AP threshold and decreasing AP amplitude (Figure 7j–m). The effects of carvedilol on single APs may result from its effects on voltage-gated sodium channels. For example, carvedilol blocks **Na_v1.6** sodium channel, which is essential for the initiation and propagation of action potentials (Atkin et al., 2018; Bean, 2007). Besides, carvedilol acts on α_1 - and β -adrenoceptors, which regulate AP hyperpolarization. For example, activation of **β_3 -adrenoceptors** suppressed mAHP in hippocampal CA1 pyramidal neurons (Church et al., 2019). In addition, **β_2 -adrenoceptors** interact with **large-conductance voltage and Ca²⁺-activated potassium channels (BK_{Ca})** and upregulate BK channel activities, which contributes to fAHP in hippocampal CA1 pyramidal neurons (Liu et al., 2004). The effects of carvedilol on adrenoceptors may modulate AHP and neuronal excitabilities of hippocampal CA1 pyramidal neurons. Therefore, carvedilol may exert anti-epileptic effects by acting on other ion channels or GPCRs. To elucidate the specific mechanism of action of carvedilol's anti-epileptic effects, further research needs to be conducted in gene knockout mice, for example, α - or β -adrenoceptor KO mice and Na_v1.6 KO mice. At the same time, carvedilol has a low IC₅₀ value for **HERG channels** (10.4 μ M) (Karle et al., 2001), making it safer than quinidine for the treatment of *KCNT1*-related epilepsies. Moreover, carvedilol is a cationic amphiphilic compound with high lipophilicity, which enables it to penetrate the blood–brain barrier (BBB) (Beaman et al., 2023). In addition to mice with *KCNT1* mutation-related epilepsy, we found that carvedilol can also markedly reduce the excitability of wild-type CA1 pyramidal neurons, thereby reducing the epileptic susceptibility in wild-type mice. This suggests that carvedilol may also have therapeutic effects in other types of epilepsy and this compound might be a new potential candidate for the treatment of several forms of epilepsy.

Here, M267T, a heterozygous *KCNT1* mutation, was found in a patient with EIMFS. This variant has been previously reported in a patient with ADNFLE (Meng et al., 2017). *KCNT1*-related epilepsy is commonly associated with the following two distinct phenotypes: EIMFS and ADNFLE. Increasing incidence of epilepsy cases suggests that one identical *KCNT1* mutation can generate a number of diverse

epilepsy phenotypes, with some variants participating in both EIMFS and ADNFLE, such as G288S, R398Q, R474C and A934T. This may be due to individual differences in their genetic and epigenetic background.

All the experiments in this project were carried out in male mice. Female mice experience hormonal fluctuations due to their oestrous cycle, which can potentially influence the consistency and reproducibility of experimental results. Future studies in mice of both sexes are necessary to provide a more comprehensive understanding of carvedilol's anti-epileptic effect.

In conclusion, the heterozygous *KCNT1* mutation, M267T, exhibits GOF channel properties, causing epilepsy by enhancing neuronal excitability. Carvedilol is an FDA-approved compound, and it can markedly reduce M267T Slack currents and neuronal excitability. Here, we have shown that carvedilol reduced the seizure susceptibility in the mouse model of epilepsy induced by kainic acid. Taken together, these findings suggest carvedilol as a promising therapeutic candidate for treating epilepsies.

AUTHOR CONTRIBUTIONS

Chang Di performed and analysed voltage-clamp recordings. Tong Wu, Huifang Song and Na Li performed and analysed molecular cloning and current-clamp recordings. Kai Gao and Yuwu Jiang collected and analysed patient information. Haojie Sun and Mala Shah performed and analysed current-clamp recordings. Jingyun Yi and Xinran Zhang performed in utero electroporation. Chang Di, Lili Wang and Jiexin Chen performed and analysed Western blotting. Zhuo Huang, Chang Di, Yuwu Jiang and Mala Shah designed the experiments. Chang Di, Tong Wu, Kai Gao and Na Li wrote the manuscript. Zhuo Huang, Yuwu Jiang and Mala Shah reviewed the manuscript.

ACKNOWLEDGEMENTS

This work was supported by Chinese National Programs for Brain Science and Brain-like intelligence technology No.2021ZD0202102 to Z. H.; National Natural Science Foundation of China Grant (Nos. 31871083 and 81371432 to Z. H.; U22A20339 and 81971211 to Y. W. J.; Nos. 82171435 to K. G.); Beijing Natural Science Foundation (No. 7212109 to K. G.); National Key Research and Development Program of China (No. 2020YFA0804000 to Y. W. J.); Key Project of Clinical Medicine Research of National Clinical Research Center for Child Health and Disorders, Children's Hospital of Chongqing Medical University (No. NCRCCHD-2021-KP-02 to Y. W. J.).

CONFLICT OF INTEREST STATEMENT

There are no conflicts of interest for any of the authors.

DATA AVAILABILITY STATEMENT

The data that support the findings of this study are available from the corresponding author upon reasonable request. Some data may not be made available because of privacy or ethical restrictions.

DECLARATION OF TRANSPARENCY AND SCIENTIFIC RIGOUR

This Declaration acknowledges that this paper adheres to the principles for transparent reporting and scientific rigour of preclinical research as stated in the *BJP* guidelines for [Design and Analysis](#), [Immunoblotting and Immunochemistry](#), and [Animal Experimentation](#), and as recommended by funding agencies, publishers and other organizations engaged with supporting research.

ORCID

Zhuo Huang  <https://orcid.org/0000-0001-9198-4778>

REFERENCES

- Alexander, S. P. H., Christopoulos, A., Davenport, A. P., Kelly, E., Mathie, A. A., Peters, J. A., Veale, E. L., Armstrong, J. F., Faccenda, E., Harding, S. D., Davies, J. A., Abbracchio, M. P., Abraham, G., Agoulnik, A., Alexander, W., Al-Hosaini, K., Bäck, M., Baker, J. G., Barnes, N. M., ... Ye, R. D. (2023). The Concise Guide to PHARMACOLOGY 2023/24: G protein-coupled receptors. *British Journal of Pharmacology*, 180(Suppl 2), S23–S144. <https://doi.org/10.1111/bph.16177>
- Alexander, S. P. H., Mathie, A. A., Peters, J. A., Veale, E. L., Striessnig, J., Kelly, E., Armstrong, J. F., Faccenda, E., Harding, S. D., Davies, J. A., Aldrich, R. W., Attali, B., Baggetta, A. M., Becirovic, E., Biel, M., Bill, R. M., Caceres, A. I., Catterall, W. A., Conner, A. C., ... Zhu, M. (2023). The Concise Guide to PHARMACOLOGY 2023/24: Ion channels. *British Journal of Pharmacology*, 180(Suppl 2), S145–S222. <https://doi.org/10.1111/bph.16181>
- Aréchiga, I. A., Barrio-Echavarría, G. F., Rodríguez-Menchaca, A. A., Moreno-Galindo, E. G., Decher, N., Tristani-Firouzi, M., Sánchez-Chapula, J. A., & Navarro-Polanco, R. A. (2008). Kv1.5 open channel block by the antiarrhythmic drug disopyramide: Molecular determinants of block. *Journal of Pharmacological Sciences*, 108(1), 49–55. <https://doi.org/10.1254/jphs.08084fp>
- Arrieta-Cruz, I., Wang, J., Pavlides, C., & Pasinetti, G. M. (2010). Carvedilol reestablishes long-term potentiation in a mouse model of Alzheimer's disease. *Journal of Alzheimer's Disease: JAD*, 21(2), 649–654. <https://doi.org/10.3233/JAD-2010-100225>
- Atkin, T. A., Maher, C. M., Gerlach, A. C., Gay, B. C., Antonio, B. M., Santos, S. C., Padilla, K. M., Rader, J., Krafte, D. S., Fox, M. A., Stewart, G. R., Petrovski, S., Devinsky, O., Might, M., Petrou, S., & Goldstein, D. B. (2018). A comprehensive approach to identifying repurposed drugs to treat SCN8A epilepsy. *Epilepsia*, 59(4), 802–813. <https://doi.org/10.1111/epi.14037>
- Barcia, G., Fleming, M. R., Deligniere, A., Gazula, V.-R., Brown, M. R., Langouet, M., Chen, H., Kronengold, J., Abhyankar, A., Cilio, R., Nitschke, P., & Nabhout, R. (2012). De novo gain-of-function KCNT1 channel mutations cause malignant migrating partial seizures of infancy. *Nature Genetics*, 44(11), 1255–1259. <https://doi.org/10.1038/ng.2441>
- Beaman, E. E., Bonde, A. N., Larsen, S. M. U., Ozenne, B., Lohela, T. J., Nedergaard, M., Gislason, G. H., Knudsen, G. M., Holst, S. C., & Holst, S. C. (2023). Blood-brain barrier permeable β -blockers linked to lower risk of Alzheimer's disease in hypertension. *Brain: a Journal of Neurology*, 146(3), 1141–1151. <https://doi.org/10.1093/brain/awac076>
- Bean, B. P. (2007). The action potential in mammalian central neurons. *Nature Reviews Neuroscience*, 8(6), 451–465. <https://doi.org/10.1038/nrn2148>
- Bearden, D., Strong, A., Ehnot, J., DiGiiovine, M., Dlugos, D., & Goldberg, E. M. (2014). Targeted treatment of migrating partial seizures of infancy with quinidine. *Annals of Neurology*, 76(3), 457–461. <https://doi.org/10.1002/ana.24229>
- Ben-Ari, Y., & Cossart, R. (2000). Kainate, a double agent that generates seizures: Two decades of progress. *Trends in Neurosciences*, 23(11), 580–587. [https://doi.org/10.1016/s0166-2236\(00\)01659-3](https://doi.org/10.1016/s0166-2236(00)01659-3)
- Bhattacharjee, A., Gan, L., & Kaczmarek, L. K. (2002). Localization of the slack potassium channel in the rat central nervous system. *The Journal of Comparative Neurology*, 454(3), 241–254. <https://doi.org/10.1002/cne.10439>
- Champéroux, P., Fares, R., Bastogne, T., Richard, S., Le Guennec, J.-Y., & Thireau, J. (2022). Contribution of haemodynamic side effects and associated autonomic reflexes to ventricular arrhythmias triggering by torsadogenic hERG blocking drugs. *British Journal of Pharmacology*, 179(18), 4549–4562. <https://doi.org/10.1111/bph.15905>
- Cheng, N., Ren, S., Yang, J.-F., Liu, X.-M., & Li, X.-T. (2019). Carvedilol blockage of delayed rectifier Kv2.1 channels and its molecular basis. *European Journal of Pharmacology*, 855, 50–55. <https://doi.org/10.1016/j.ejphar.2019.05.006>
- Church, T. W., Brown, J. T., & Marrion, N. V. (2019). β 3-adrenergic receptor-dependent modulation of the medium afterhyperpolarization in rat hippocampal CA1 pyramidal neurons. *Journal of Neurophysiology*, 121(3), 773–784. <https://doi.org/10.1152/jn.00334.2018>
- Cioclu, M. C., Mosca, I., Ambrosino, P., Puzo, D., Bayat, A., Wortmann, S. B., Koch, J., Strehlow, V., Shirai, K., Matsumoto, N., Sanders, S. J., & Tagliatalata, M. (2023). KCNT2-related disorders: Phenotypes, functional, and pharmacological properties. *Annals of Neurology*, 94(2), 332–349. <https://doi.org/10.1002/ana.26662>
- Coppola, G., Plouin, P., Chiron, C., Robain, O., & Dulac, O. (1995). Migrating partial seizures in infancy: A malignant disorder with developmental arrest. *Epilepsia*, 36(10), 1017–1024. <https://doi.org/10.1111/j.1528-1157.1995.tb00961.x>
- Dong, D.-L., Wang, Q.-H., Yue, P., Jiao, J.-D., Gu, R.-M., & Yang, B.-F. (2006). Indapamide induces apoptosis of GH3 pituitary cells independently of its inhibition of voltage-dependent K⁺ currents. *European Journal of Pharmacology*, 536(1–2), 78–84. <https://doi.org/10.1016/j.ejphar.2006.02.037>
- Dopp, A. L., Miller, J. M., & Tisdale, J. E. (2008). Effect of drugs on defibrillation capacity. *Drugs*, 68(5), 607–630. <https://doi.org/10.2165/00003495-200868050-00004>
- Du, X., Carvalho-de-Souza, J. L., Wei, C., Carrasquel-Ursulaez, W., Lorenzo, Y., Gonzalez, N., Kubota, T., Staisch, J., Hain, T., Petrossian, N., Xu, M., & Gomez, C. M. (2020). Loss-of-function BK channel mutation causes impaired mitochondria and progressive cerebellar ataxia. *Proceedings of the National Academy of Sciences of the United States of America*, 117(11), 6023–6034. <https://doi.org/10.1073/pnas.1920008117>
- Ei-Sherif, N., & Turitto, G. (2005). Electrophysiologic effects of carvedilol: Is carvedilol an antiarrhythmic agent? *Pacing and Clinical Electrophysiology: PACE*, 28(9), 985–990. <https://doi.org/10.1111/j.1540-8159.2005.00200.x>
- Franceschetti, S., Lavazza, T., Curia, G., Aracri, P., Panzica, F., Sancini, G., Avanzini, G., & Magistretti, J. (2003). Na⁺-activated K⁺ current contributes to postexcitatory hyperpolarization in neocortical intrinsically bursting neurons. *Journal of Neurophysiology*, 89(4), 2101–2111. <https://doi.org/10.1152/jn.00695.2002>
- Gao, S.-B., Wu, Y., Lü, C.-X., Guo, Z.-H., Li, C.-H., & Ding, J.-P. (2008). Slack and slick KNa channels are required for the depolarizing afterpotential of acutely isolated, medium diameter rat dorsal root ganglion neurons. *Acta Pharmacologica Sinica*, 29(8), 899–905. <https://doi.org/10.1111/j.1745-7254.2008.00842.x>
- Gomma, A. H., Purcell, H. J., & Fox, K. M. (2001). Potassium channel openers in myocardial ischaemia: Therapeutic potential of nicorandil. *Drugs*, 61(12), 1705–1710. <https://doi.org/10.2165/00003495-200161120-00002>

- Heron, S. E., Smith, K. R., Bahlo, M., Nobili, L., Kahana, E., Licchetta, L., Oliver, K. L., Mazarib, A., Afawi, Z., Korczyn, A., Plazzi, G., & Dibbens, L. M. (2012). Missense mutations in the sodium-gated potassium channel gene *KCNT1* cause severe autosomal dominant nocturnal frontal lobe epilepsy. *Nature Genetics*, 44(11), 1188–1190. <https://doi.org/10.1038/ng.2440>
- Hess, D., Nanou, E., & El Manira, A. (2007). Characterization of Na⁺-activated K⁺ currents in larval lamprey spinal cord neurons. *Journal of Neurophysiology*, 97(5), 3484–3493. <https://doi.org/10.1152/jn.00742.2006>
- Huang, Z., Lujan, R., Kadurin, I., Uebele, V. N., Renger, J. J., Dolphin, A. C., & Shah, M. M. (2011). Presynaptic HCN1 channels regulate Cav3.2 activity and neurotransmission at select cortical synapses. *Nature Neuroscience*, 14(4), 478–486. <https://doi.org/10.1038/nn.2757>
- Ishii, A., Shioda, M., Okumura, A., Kidokoro, H., Sakauchi, M., Shimada, S., Shimizu, T., Osawa, M., Hirose, S., & Yamamoto, T. (2013). A recurrent *KCNT1* mutation in two sporadic cases with malignant migrating partial seizures in infancy. *Gene*, 531(2), 467–471. <https://doi.org/10.1016/j.gene.2013.08.096>
- Karle, C. A., Kreye, V. A., Thomas, D., Röckl, K., Kathöfer, S., Zhang, W., & Kiehn, J. (2001). Antiarrhythmic drug carvedilol inhibits HERG potassium channels. *Cardiovascular Research*, 49(2), 361–370. [https://doi.org/10.1016/s0008-6363\(00\)00265-0](https://doi.org/10.1016/s0008-6363(00)00265-0)
- Kim, G. E., Kronengold, J., Barcia, G., Quraishi, I. H., Martin, H. C., Blair, E., Taylor, J. C., Dulac, O., Colleaux, L., Nabbout, R., & Kaczmarek, L. K. (2014). Human slack potassium channel mutations increase positive cooperativity between individual channels. *Cell Reports*, 9(5), 1661–1672. <https://doi.org/10.1016/j.celrep.2014.11.015>
- King, B., Rizwan, A. P., Asmara, H., Heath, N. C., Engbers, J. D. T., Dykstra, S., Bartoletti, T. M., Hameed, S., Zamponi, G. W., & Turner, R. W. (2015). IKCa channels are a critical determinant of the slow AHP in CA1 pyramidal neurons. *Cell Reports*, 11(2), 175–182. <https://doi.org/10.1016/j.celrep.2015.03.026>
- Kuchenbuch, M., Barcia, G., Chemaly, N., Carme, E., Roubertie, A., Gibaud, M., Van Bogaert, P., de Saint Martin, A., Hirsch, E., Dubois, F., Sarret, C., & Nabbout, R. (2019). *KCNT1* epilepsy with migrating focal seizures shows a temporal sequence with poor outcome, high mortality and SUDEP. *Brain: a Journal of Neurology*, 142(10), 2996–3008. <https://doi.org/10.1093/brain/awz240>
- León-Ruiz, M., Alonso-Singer, P., Merino-Andreu, M., & Castañeda-Cabrero, C. (2024). A challenging case of epilepsy in infancy with migrating focal seizures due to a de novo *KCNT1* missense variant (c.1438G>a, p.Asp480Asn). *Seizure*, 117, 202–205. <https://doi.org/10.1016/j.seizure.2024.02.020>
- Lilley, E., Stanford, S. C., Kendall, D. E., Alexander, S. P. H., Cirino, G., Docherty, J. R., George, C. H., Insel, P. A., Izzo, A. A., Ji, Y., Panettieri, R. A., Sobey, C. G., Stefanska, B., Stephens, G., Teixeira, M. M., & Ahluwalia, A. (2020). ARRIVE 2.0 and the British Journal of Pharmacology: Updated guidance for 2020. *British Journal of Pharmacology*, 177, 3611–3616. <https://doi.org/10.1111/bph.15178>
- Liu, G., Shi, J., Yang, L., Cao, L., Park, S. M., Cui, J., & Marx, S. O. (2004). Assembly of a Ca²⁺-dependent BK channel signaling complex by binding to beta2 adrenergic receptor. *The EMBO Journal*, 23(11), 2196–2205. <https://doi.org/10.1038/sj.emboj.7600228>
- Liu, X., & Stan Leung, L. (2004). Sodium-activated potassium conductance participates in the depolarizing afterpotential following a single action potential in rat hippocampal CA1 pyramidal cells. *Brain Research*, 1023(2), 185–192. <https://doi.org/10.1016/j.brainres.2004.07.017>
- Lu, R., Bausch, A. E., Kallenborn-Gerhardt, W., Stoetzer, C., Debruin, N., Ruth, P., Geisslinger, G., Leffler, A., Lukowski, R., & Schmidtko, A. (2015). Slack channels expressed in sensory neurons control neuropathic pain in mice. *The Journal of Neuroscience: the Official Journal of the Society for Neuroscience*, 35(3), 1125–1135. <https://doi.org/10.1523/JNEUROSCI.2423-14.2015>
- Lysko, P. G., Lysko, K. A., Yue, T. L., Webb, C. L., Gu, J. L., & Feuerstein, G. (1992). Neuroprotective effects of carvedilol, a new antihypertensive agent, in cultured rat cerebellar neurons and in gerbil global brain ischemia. *Stroke*, 23(11), 1630–1635. <https://doi.org/10.1161/01.STR.23.11.1630>
- Martin, H. C., Kim, G. E., Pagnamenta, A. T., Murakami, Y., Carvill, G. L., Meyer, E., Copley, R. R., Rimmer, A., Barcia, G., Fleming, M. R., Kronengold, J., & Taylor, J. C. (2014). Clinical whole-genome sequencing in severe early-onset epilepsy reveals new genes and improves molecular diagnosis. *Human Molecular Genetics*, 23(12), 3200–3211. <https://doi.org/10.1093/hmg/ddu030>
- Martinez-Espinosa, P. L., Wu, J., Yang, C., Gonzalez-Perez, V., Zhou, H., Liang, H., Liang, H., Xia, X. M., & Lingle, C. J. (2015). Knockout of *Slo2.2* enhances itch, abolishes KNa current, and increases action potential firing frequency in DRG neurons. *eLife*, 4, e10013. <https://doi.org/10.7554/eLife.10013>
- Meng, L., Pammi, M., Saronwala, A., Magoulas, P., Ghazi, A. R., Vetrini, F., Zhang, J., He, W., Dharmadhikari, A. V., Qu, C., Ward, P., & Lalani, S. R. (2017). Use of exome sequencing for infants in intensive care units: Ascertainment of severe single-gene disorders and effect on medical management. *JAMA Pediatrics*, 171(12), e173438. <https://doi.org/10.1001/jamapediatrics.2017.3438>
- Mikati, M. A., Jiang, Y.-H., Carboni, M., Shashi, V., Petrovski, S., Spillmann, R., Milligan, C. J., Li, M., Grefe, A., McConkie, A., Berkovic, S., & Goldstein, D. (2015). Quinidine in the treatment of *KCNT1*-positive epilepsies. *Annals of Neurology*, 78(6), 995–999. <https://doi.org/10.1002/ana.24520>
- Milligan, C. J., Li, M., Gazina, E. V., Heron, S. E., Nair, U., Trager, C., Reid, C. A., Venkat, A., Younkin, D. P., Dlugos, D. J., Petrovski, S., & Petrou, S. (2014). *KCNT1* gain of function in 2 epilepsy phenotypes is reversed by quinidine. *Annals of Neurology*, 75(4), 581–590. <https://doi.org/10.1002/ana.24128>
- Møller, R. S., Heron, S. E., Larsen, L. H. G., Lim, C. X., Ricos, M. G., Bayly, M. A., Van Kempen, M. J., Klinkenberg, S., Andrews, I., Kelley, K., Ronen, G. M., & Dibbens, L. M. (2015). Mutations in *KCNT1* cause a spectrum of focal epilepsies. *Epilepsia*, 56(9), e114–e120. <https://doi.org/10.1111/epi.13071>
- Mullen, S. A., Carney, P. W., Roten, A., Ching, M., Lightfoot, P. A., Churilov, L., Nair, U., Li, M., Berkovic, S. F., Petrou, S., & Scheffer, I. E. (2018). Precision therapy for epilepsy due to *KCNT1* mutations: A randomized trial of oral quinidine. *Neurology*, 90(1), e67–e72. <https://doi.org/10.1212/WNL.0000000000004769>
- Numis, A. L., Nair, U., Datta, A. N., Sands, T. T., Oldham, M. S., Patel, A., Li, M., Gazina, E., Petrou, S., & Cilio, M. R. (2018). Lack of response to quinidine in *KCNT1*-related neonatal epilepsy. *Epilepsia*, 59(10), 1889–1898. <https://doi.org/10.1111/epi.14551>
- Ohba, C., Kato, M., Takahashi, N., Osaka, H., Shiihara, T., Tohyama, J., Nabatame, S., Azuma, J., Fujii, Y., Hara, M., Tsurusawa, R., & Matsumoto, N. (2015). De novo *KCNT1* mutations in early-onset epileptic encephalopathy. *Epilepsia*, 56(9), e121–e128. <https://doi.org/10.1111/epi.13072>
- Patel, C., Yan, G.-X., & Kowey, P. R. (2009). Dronedrone. *Circulation*, 120(7), 636–644. <https://doi.org/10.1161/CIRCULATIONAHA.109.858027>
- Percie du Sert, N., Hurst, V., Ahluwalia, A., Alam, S., Avey, M. T., Baker, M., Browne, W. J., Clark, A., Cuthill, I. C., Dirnagl, U., Emerson, M., Garner, P., Holgate, S. T., Howells, D. W., Karp, N. A., Lazic, S. E., Lidster, K., MacCallum, C. J., Macleod, M., ... Würbel, H. (2020). The ARRIVE guidelines 2.0: updated guidelines for reporting animal research. *PLoS Biol*, 18, e3000410. <https://doi.org/10.1371/journal.pbio.3000410>
- Quraishi, I. H., Mercier, M. R., McClure, H., Couture, R. L., Schwartz, M. L., Lukowski, R., Ruth, P., & Kaczmarek, L. K. (2020). Impaired motor skill learning and altered seizure susceptibility in mice with loss or gain of

- function of the *Kcnt1* gene encoding slack (KNa1.1) Na⁺-activated K⁺ channels. *Scientific Reports*, 10(1), 3213. <https://doi.org/10.1038/s41598-020-60028-z>
- Quraishi, I. H., Stern, S., Mangan, K. P., Zhang, Y., Ali, S. R., Mercier, M. R., Marchetto, M. C., McLachlan, M. J., Jones, E. M., Gage, F. H., & Kaczmarek, L. K. (2019). An epilepsy-associated KCNT1 mutation enhances excitability of human iPSC-derived neurons by increasing slack KNa currents. *The Journal of Neuroscience: the Official Journal of the Society for Neuroscience*, 39(37), 7438–7449. <https://doi.org/10.1523/JNEUROSCI.1628-18.2019>
- Racine, R. J. (1972). Modification of seizure activity by electrical stimulation. II. Motor seizure. *Electroencephalography and Clinical Neurophysiology*, 32(3), 281–294. [https://doi.org/10.1016/0013-4694\(72\)90177-0](https://doi.org/10.1016/0013-4694(72)90177-0)
- Sahu, G., & Turner, R. W. (2021). The molecular basis for the calcium-dependent slow Afterhyperpolarization in CA1 hippocampal pyramidal neurons. *Frontiers in Physiology*, 12, 759707. <https://doi.org/10.3389/fphys.2021.759707>
- Schwindt, P. C., Spain, W. J., & Crill, W. E. (1989). Long-lasting reduction of excitability by a sodium-dependent potassium current in cat neocortical neurons. *Journal of Neurophysiology*, 61(2), 233–244. <https://doi.org/10.1152/jn.1989.61.2.233>
- Shimada, S., Hirano, Y., Ito, S., Oguni, H., Nagata, S., Shimojima, K., & Yamamoto, T. (2014). A novel KCNT1 mutation in a Japanese patient with epilepsy of infancy with migrating focal seizures. *Human Genome Variation*, 1, 14027. <https://doi.org/10.1038/hgv.2014.27>
- Shore, A. N., Colombo, S., Tobin, W. F., Petri, S., Cullen, E. R., Dominguez, S., Bostick, C. D., Beaumont, M. A., Williams, D., Khodagholy, D., Yang, M., & Weston, M. C. (2020). Reduced GABAergic neuron excitability, altered synaptic connectivity, and seizures in a KCNT1 gain-of-function mouse model of childhood epilepsy. *Cell Reports*, 33(4), 108303. <https://doi.org/10.1016/j.celrep.2020.108303>
- Sindrup, S. H., Hofmann, U., Asmussen, J., Mikus, G., Brøsen, K., Nielsen, F., Ingwersen, S. H., & Broen Christensen, C. (1996). Impact of quinidine on plasma and cerebrospinal fluid concentrations of codeine and morphine after codeine intake. *European Journal of Clinical Pharmacology*, 49(6), 503–509. <https://doi.org/10.1007/bf00195938>
- Tabata, H., & Nakajima, K. (2001). Efficient in utero gene transfer system to the developing mouse brain using electroporation: Visualization of neuronal migration in the developing cortex. *Neuroscience*, 103(4), 865–872. [https://doi.org/10.1016/s0306-4522\(01\)00016-1](https://doi.org/10.1016/s0306-4522(01)00016-1)
- Wu, J., El-Hassar, L., Datta, D., Thomas, M., Zhang, Y., Jenkins, D. P., DeLuca, N. J., Chatterjee, M., Gribkoff, V. K., Arnsten, A. F., & Kaczmarek, L. K. (2024). Interaction between HCN and slack channels regulates mPFC pyramidal cell excitability in working memory circuits. *Molecular Neurobiology*, 61(4), 2430–2445. <https://doi.org/10.1007/s12035-023-03719-8>
- Wulff, H., Castle, N. A., & Pardo, L. A. (2009). Voltage-gated potassium channels as therapeutic targets. *Nature Reviews. Drug Discovery*, 8(12), 982–1001. <https://doi.org/10.1038/nrd2983>
- Yang, B., Desai, R., & Kaczmarek, L. K. (2007). Slack and slick K (Na) channels regulate the accuracy of timing of auditory neurons. *The Journal of Neuroscience: the Official Journal of the Society for Neuroscience*, 27(10), 2617–2627. <https://doi.org/10.1523/JNEUROSCI.5308-06.2007>
- Yang, J. F., Cheng, N., Ren, S., Liu, X. M., & Li, X. T. (2018). Characterization and molecular basis for the block of Kv1.3 channels induced by carvedilol in HEK293 cells. *European Journal of Pharmacology*, 834, 206–212. <https://doi.org/10.1016/j.ejphar.2018.07.025>
- Yuan, A., Santi, C. M., Wei, A., Wang, Z. W., Pollak, K., Nonet, M., Kaczmarek, L., Crowder, C. M., & Salkoff, L. (2003). The sodium-activated potassium channel is encoded by a member of the Slo gene family. *Neuron*, 37(5), 765–773. [https://doi.org/10.1016/s0896-6273\(03\)00096-5](https://doi.org/10.1016/s0896-6273(03)00096-5)
- Yuan, T., Wang, Y., Jin, Y., Yang, H., Xu, S., Zhang, H., Chen, Q., Li, N., Ma, X., Song, H., Peng, C., & Huang, Z. (2024). Coupling of slack and Na(V)1.6 sensitizes slack to quinidine blockade and guides anti-seizure strategy development. *eLife*, 12, RP87559. <https://doi.org/10.7554/eLife.87559>

SUPPORTING INFORMATION

Additional supporting information can be found online in the Supporting Information section at the end of this article.

How to cite this article: Di, C., Wu, T., Gao, K., Li, N., Song, H., Wang, L., Sun, H., Yi, J., Zhang, X., Chen, J., Shah, M., Jiang, Y., & Huang, Z. (2024). Carvedilol inhibits neuronal hyperexcitability caused by epilepsy-associated KCNT1 mutations. *British Journal of Pharmacology*, 1–19. <https://doi.org/10.1111/bph.17360>